Enlightening the Alkali Ion Role in the Photomagnetic Effect of FeCo Prussian Blue Analogues

Jana Glatz, Juan-Ramón Jiménez, Louis Godeffroy, Hans Jurgen von Bardeleben, Laure Fillaud, Emmanuel Maisonhaute, Yanling Li, Lise-Marie Chamoreau, Rodrigue Lescouëzec

Enlightening the Alkali Ion Role on the Photomagnetic Effect of FeCo Prussian Blue Analogues

Jana Glatz,[‡a] Juan-Ramon Jiménez,[‡a] Louis Godeffroy,[b] Hans Jurgen von Bardeleben,[c] Laure Fillaud,[b] Emmanuel Maisonhaute,[b] Yanling Li,[a] Lise-Marie Chamoreau,[a] Rodrigue Lescouëzec*[a]

[a]Institut Parisien de Chimie Moléculaire, CNRS UMR 8232, Sorbonne Université, 4 place Jussieu F-75252 Paris cedex5

[b]Laboratoire Interface et Systèmes Electrochimiques, CNRS UMR 8235, Sorbonne Université, 4 place Jussieu F-75252 Paris cedex5

[c]Institut des Nanosciences de Paris, CNRS UMR 7588, Sorbonne Université, 4 place Jussieu F-75252 Paris cedex5

KEYWORDS: Molecular Switch, Charge Transfer, Photomagnetism, Prussian Blue Analogues, Cyanide.

ABSTRACT: Fe-Co Prussian blue analogues of general formula $A_xCo_y[Fe(CN)_6]_z$ are responsive, non-stoichiometric materials whose magnetic and optical properties can be reversibly switched by light irradiation. However, elucidating the critical influence of the inserted alkali ion, A^+, on the material's properties remains complicated due to their complex local structure. Here, by investigating soluble $A\subset[Fe_4\text{-}Co_4]$ cyanido cubes (A = K, Rb and Cs), both accurate structural and electronic information could be obtained. Firstly, XRD analyses reveal distinct interactions between the inserted A^+ ions and the $\{Fe_4\text{-}Co_4\}$ box, which impact the structural distortion in the cubic framework. These distortions vanish and a displacement of the small K^+ ion from a corner toward the center is observed as a cobalt corner Co^{II}_{HS} is oxidized to Co^{III}_{LS}. Secondly, cyclic voltammetry experiments performed at variable temperatures show distinct splitting of the $Co^{II}_{HS} \Leftrightarrow Co^{III}_{LS}$ peak potentials for the different A^+ cations, which can be qualitatively linked to different thermodynamic (standard potentials) and kinetic (energy barriers) parameters associated with the structural reorganization accompanying this redox coupled spin state change. Moreover, for the first time, photo-magnetism was investigated in frozen solution to avoid effects of intermolecular interactions. The results show that the metastable state is stabilized following the trend K > Rb > Cs. The outcome of these studies suggests that the interaction of the inserted alkali ions with the cyanide cage and the structural changes accompanying the electron transfer impact the stability of the photo-induced state and the relaxation temperature: the smaller the cation, the higher the structural reorganization and the associated energy barrier, and the more stable the metastable state.

INTRODUCTION

The possibility of controlling and manipulating the electronic properties of a material by an external stimulus is an attractive challenge in material science. In this context, photomagnetic materials showing light-induced modifications of their magnetic and optical properties are the object of study for both fundamental aspects and potential applications.[1,2] On the one hand, efforts are focused on understanding the origin of the photo-magnetic phenomenon on the molecular level. On the other hand, applied research deals with the integration of these photo-magnets into original functional materials.[3–7] An important class of photomagnetic systems are the charge-transfer (CT) complexes, which show a reversible electron transfer between a ligand and a metal or between two metal ions linked by a bridging ligand.[8,2,9] The origin of these phenomena lies in the coexistence of two different electronic states that are close in energy, which can be reversibly interconverted into each other by applying an external stimulus such as a light irradiation, a change of temperature, pressure or an electric field.[2,10] The light stimulus is particularly interesting because it can be fast, localized and its energy is tunable by the choice of the irradiation wavelength. It was in 1996, that Sato *et al.* published the first photo-magnetic material based on a metal-metal electron transfer: an FeCo Prussian blue analogue (PBA) of formula $K_{0.2}Co_{1.4}[Fe(CN)_6]\cdot 6.9H_2O$.[11] In this material, a light irradiation at low temperature induces an Electron Transfer Coupled Spin Transition (ETCST) on the cobalt, converting thus diamagnetic Fe^{II}_{LS}-CN-Co^{III}_{LS} pairs into paramagnetic Fe^{III}_{LS}-CN-Co^{II}_{HS} (LS = low-spin and HS = high spin) ones. Actually, only very recently Collet *et al.* showed that it is the light-induced spin-transition that triggers the electron transfer.[12] Since the seminal result of Sato *et al.*, continuous efforts have been devoted to better understand and improve the performance of the photomagnetic FeCo PBAs. This task is complicated due to the complex local structure of PBAs. Indeed PBAs, of general formula $A_xM'_4[M(CN)_6]_{(8+x)/3}[]_{(4-x)/3}\cdot nH_2O$, are non-stoichiometric inorganic polymers, which contain a variable amount of $[M(CN)_6]$ vacancies (noted []) and inserted cations A^+). Solid NMR studies have shown, that different kind of vacancies and different metal sites, $\{M'(NC)_{6-n}(H_2O)_n\}$, coexist in the same PBA.[13–15] The macroscopic properties of FeCo PBA thus result from the interaction of a diversity of {Fe-CN-Co} pairs showing different local surroundings. In the last two decades, in depth investigations and systematic studies of several series of FeCo PBAs showed that the photomagnetic effect critically depends on various interconnected structural and electronic

parameters, such as: the ligand field and the redox potential of the Co atom, the bending of the cyanide-bridge as well as the flexibility of the network. Interestingly, it was observed that the amount and the nature of the inserted alkali ions have a strong impact on these parameters.[16–19] First of all, it was shown that the presence of alkali ions is necessary to obtain switchable Fe^{II}_{LS}-CN-Co^{III}_{LS} ⇔ Fe^{III}_{LS}-CN-Co^{II}_{HS} pairs in the FeCo PBA.[19] Furthermore, the amount of the inserted ions is linked to the occurrence of vacancies, which in turn control the cobalt coordination sphere $\{Co(NC)_{6-n}(H_2O)_n\}$. The latter influences the ligand field of the Co ions and subsequently the electron-transfer properties.[17,20] However, the insertion of a large amount of ions (and the consequently low amount of vacancies) is believed to confer some stiffness to the three-dimensional network, thus preventing the structural reorganization accompanying the electron transfer.[17,21] This would account for the absence of the photomagnetic effect in the $Cs_4Co_4[Fe(CN)_6]_4$ PBA that has no vacancies and where Cs^+ ions fully occupy the cavity of the network. In contrast, $Cs_{0.7}Co_4[Fe(CN)_6]_{2.9}$ was shown to be an efficient photomagnetic PBA.[19] In this particular case, the photo-switching is accompanied by a displacement of the Cs^+ ion toward a vacancy.[22] The interaction of the alkali ion with the cyanide-π system is also believed to affect the CN-Co linkage and consequently the electronic properties of the Co ions and in particular their redox potential.[20] Besides the intrinsic composition of the material other factors such as the size of the PBA (nano)particles were shown to affect the photomagnetic behaviour.[23–26]

Another way to address the rationalization of the photomagnetic properties is to design low dimensional models of PBAs where structural and electronic parameters can be better adjusted and controlled.[9,27,28] For example, two studies by Nihei *et al.*[29] and Zhang *et al.*[30] which each investigated a series of cyanide-based $\{Fe_2Co_2\}$ square complexes showed that the donor ability of the ancillary ligands could be correlated to the redox potentials of the metal components and thus to the electron transfer properties. As postulated for FeCo PBAs, the reversible ETCST can only occur if the Fe^{III}/Fe^{II} and Co^{III}/Co^{II} redox couples are close enough or, in other words, if the Gibbs energy variation, ΔG, associated with the metal-metal charge transfer reaction $Fe^{II}Co^{III}$ ⇔ $Fe^{III}Co^{II}$ is moderate. In such case, a thermal variation can lead to a full compensation of the enthalpy contribution, ΔH, by the entropic-dependent term, TΔS, leading to a changeover of the ground state at the transition temperature, $T_{1/2}$. Thus $T_{1/2}$ is the temperature at which both states $Fe^{III}Co^{II}$ and $Fe^{II}Co^{III}$ coexist in equal amount. A recent study established a clear correlation between the differences in the $Fe^{III/II}$ and $Co^{III/II}$ redox potentials and the transition temperatures, $T_{1/2}$ measured in solution.[31,32] Moreover, solution studies on soluble $\{Fe_2Co_2\}$ molecular models also allowed enlightening the influence of weak intermolecular interactions on the charge transfer equilibria. For example, the use of polar solvents was recognized to stabilize the more polar diamagnetic state and to shift $T_{1/2}$ to higher temperatures.[33] H-bond interactions in solution were also demonstrated to be an efficient tool in tuning the transition temperature of soluble $\{Fe_2Co_2\}$ square complexes. Here the interaction of an H-donor acid group with the non-bridging cyanide of the ferrocyanide moieties lead to a predictable increase of the $Fe^{III/II}$ redox potential and a stabilization of the diamagnetic state (*i.e.* an increase of $T_{1/2}$).[29] Rationalizing the charge-transfer equilibrium is often more difficult in the solid state. In the bulk crystalline materials, the intermolecular interactions and crystal packing, that impact the internal structure of the square and its electronic features are not always easy to predict and control. For example, several works showed that, depending on the crystal phases, the reversible charge transfer transition of the same FeCo molecular switch could be either allowed or blocked.[34–36] Although it remains challenging, recent studies have been successful in rationalizing or controlling the charge transfer transition trough supramolecular approaches.[30,31,35,37]

In this context, with the aim of investigating in more depth the influence of the alkali ion on the photomagnetic effect, we initiated the study of a series of cyanido-complexes, $A\subset\{[Fe(Tp)(CN)_3)]_4[Co(pzTp)(CN)_3)]_4\}$, (abbreviated **$A\subset\{Fe_4\text{-}Co_4\}$** hereafter), which represent the elemental cubic unit of the PBA materials (A = K, Rb, Cs; Tp^- = hydrotris(pyrazol-1-yl)borate; $pzTp^-$ = tetrakis(pyrazol-1-yl)borate). We first reported the photomagnetic properties in the solid-state of the cubic complexes **$K\subset\{Fe_4\text{-}Co_4\}$** and the **$Cs\subset\{Fe_4\text{-}Co_4\}$**.[38–40] The comparison of these seminal studies could suggest that the Cs-cube shows a higher photomagnetic effect. However, as shown in this work the situation is more complicated as the switchable properties strongly depend on the crystal phase. Taking profit of the remarkable stability of these three cubes in solution, we study here for the first time the photomagnetic effects in frozen solution, in order to investigate the charge transfer at a molecular level. The kinetics of the relaxation from the metastable to the ground state allows (i) accessing the energy barrier, E_a, of the relaxation process from the metastable to the ground state for each alkali ion and, (ii) establishing an unambiguous trend $E_a(Cs) < E_a(Rb) < E_a(K)$ similar to that observed in PBAs. The confrontation of these results with structural and electronic information obtained from the single-crystal XRD analyses, the electrochemistry and EPR data allows enlightening the role of the alkali ions on the photomagnetic effect. Overall, the experimental results on "isolated" molecular models reveal the impact of the interactions between the alkali ion with the cyanide cage on the structural reorganisation, which influence itself the stabilization of the metastable state.

RESULTS AND DISCUSSION

Syntheses

The three **$A\subset\{Fe_4\text{-}Co_4\}$** compounds (A = K, Rb or Cs) were synthesized following the same procedure. Firstly, $NBu_4[Fe^{III}(Tp)(CN)_3]$, $Co(ClO_4)_2$ and $A(ClO_4)$ salts were mixed in DMF, leading to red solutions. Then a small excess of the ligand $pzTp^-$ was added, yielding a blue/green solution. The compounds, which precipitate as blue powders were washed and recrystallized in two different ways: crystals were obtained either by slow evaporation of an acetonitrile solution (phase 1), or by slow evaporation of a DMF-dichloromethane solution (phase 2). The isolation of two distinct crystal phases only aims at enlightening the impact of solid-state effect on the photomagnetic properties (see below and ESI). In both cases, blue rod-like crystals were obtained with yields of *ca.* 40-60 % (see details in ESI). The change of color upon addition of the $pzTp^-$ ligand (see ESI) accounts for the occurrence of an electron transfer. While the red color is typical for Fe^{III}-CN-Co^{II} pairs**,** the deep blue color is assigned to the Metal-Metal Charge Transfer in the Fe^{II}-CN-Co^{III} pair.[41] The electron transfer is driven by the substitution of coordinated solvent

molecules by the N-donor $pzTp^-$ anionic ligand, which induces a stronger ligand field on the cobalt and leads to a decrease of its redox potential. In fact the enhancement of the reducing power of the Co^{II} ion when coordinated by the $pzTp^-$ ligand can be illustrated by comparing the redox potential of the hexaaquacobaltate ($E_{1/2}$° $[Co^{III/II}(OH_2)_6]$ = 1.48 vs Fc) with the cobalt-bis[tetrakis(pyrazol-1-yl)borate) ($E_{1/2}$° $[Co^{III/II}(pzTp)_2]$ = 0.22 V in CH_2Cl_2 vs Fc). Simultaneously, the redox potential of the $[Fe^{III}(Tp)(CN)_3]^-$ units increases by coordination of a Lewis acid to the nitrogen of the cyanides.[38] Interestingly, the isolated electronic state, **A⊂{Fe^{II}_4-$Co^{III}_3Co^{II}$}**, corresponds to the neutral species in which the monoanionic charge of the cubic box is compensated by the inserted alkali ion, A^+. We assume that the precipitation of the neutral species favours the isolation of these species.

Crystal Structures

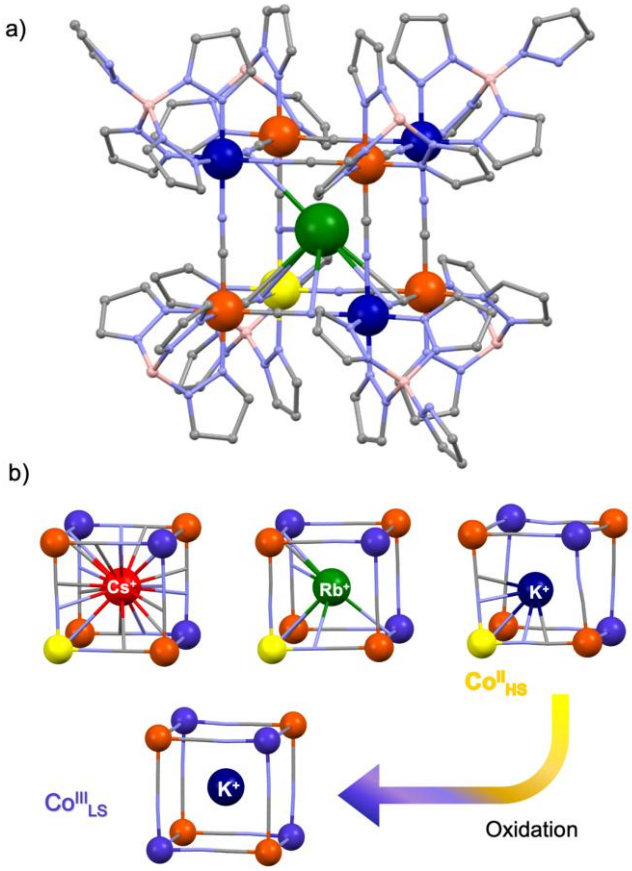

Figure 1. (a) Perspective view of the cubic complex **Rb⊂{Fe_4-Co_4}** in phase 1 (green: Rb^+, Orange Co^{III}, yellow, Co^{II}, blue Co^{III}, pink: B, light blue: N, grey: C; H are omitted). The short contacts between Rb and CN ligands are also represented as sticks. (b) Perspective view of the core structure of the cubic complexes A⊂{Fe^{II}_4-$Co^{II}_3Co^{II}$} and K⊂{Fe^{II}_4-Co^{II}_4}$^+$ showing the position of A^+ inside the cube and the A-π_{CN} interactions (short contacts between A^+ and CN appear as sticks).

All the X-ray structural data of the **A⊂{Fe_4-Co_4}** compounds were measured at 200 K. The compounds obtained in acetonitrile solution (phase 1, Figure 1) crystallize in a triclinic space group ($P\bar{1}$) while those obtained in CH_2Cl_2-DMF (phase 2) crystallize in a trigonal-space group (*R3c*). In both cases the structure is composed of cubic molecules containing an inserted alkali ion and solvate molecules. As previously described for the reported structure of **Cs⊂{Fe_4-Co_4}** in phase 1, each cube consists of four iron and four cobalt atoms that alternatively occupy the vertices of the cubes to form a heterocubane structure.[39] The Fe-CN-Co edge lengths are similar within the **A⊂{Fe_4-Co_4}** family, independently of the nature of the intercalated cation or the crystal phase, with an average distance of 4.99 Å. The volume of a cube is thus *ca.* 125 $Å^3$, leading to a van der Waals volume of 48 $Å^3$ similarly to other reported cyanide-bridged cubic cages.[42,43] Interestingly, the measured Fe-CN-Co edge length is higher than the expected value for Fe^{II}-CN-Co^{III} linkages (approximately 4.91 Å) and reflects the presence of one high-spin cobalt(II) ion (noted Co^{II}_{HS}) inside the cube. The presence of one high-spin Co^{II}_{HS} ion per cube is also clearly supported by the EPR spectra and magnetic measurements (see details in ESI). The examination of the Co-N bond lengths indicates that the Co^{II}_{HS} ion is not localized at a defined position, but it is statistically distributed between different vertices: the Co-N_{CN} average distances of each corner site thus reflect the statistical distribution of the Co^{II}_{HS} which show a Co-N bond length of *ca.* 2.10 Å in comparison to *ca.* 1.91 for the Co^{III}_{LS} (see ESI for details).

In the following discussion, the focus is set on the features that can be relevant to the distinct photomagnetic behaviors of the different phases and different alkali ions: (i) the position of the alkali ions and their interactions with the host cage {Fe_4-Co_4}; (ii) the differences in the crystal packing between the two phases. The interaction between the alkali ion and the cage is analyzed here using the crystal data of phase 1 since phase 2 shows significant disorder. Whereas the global crystal structures of **A⊂{Fe_4-Co_4}** are almost identical and independent of A, the local structure around the alkali cation and its interaction with the cage are strongly influenced by its nature. Figure 1 shows the relative position of the inserted Cs^+, Rb^+ and K^+ ion inside the {Fe_4-Co_4} host cages in phase 1. The Cs^+ ion, whose size approximately fits that of the cavity, is located almost in the center of the cage, only slightly closer to one of the cage's faces. In contrast, the smaller K^+ ion is clearly shifted towards one of the Co corners, whereas the Rb^+ ion is located in an intermediate position between the K^+ and Cs^+. These differences are reflected by the distance between the alkali ion and the cage gravity center: 0.08 Å for Cs^+, 0.15 Å for Rb^+ and *ca.* 0.43 Å for K^+. A close analysis of the structural data based on the examination of Co-N bond distances and Co-Fe edge distances (see details in ESI) reveals that the inserted cations are actually closer to the Co sites containing the Co^{II} ion (or to edges of faces containing the Co^{II} ion where the latter indicates partial occupancy over different vertices). These displacements away from the center of the cube of the inserted cations are thus ascribed to the electrostatic interaction between the cationic alkali ion and the anionic {Co^{II}(pzTp)$(NC)_3$} unit whose formal charge is -0.5 (considering the negative charge of pzTp and the negative charge of each bridging cyanide which is shared by two metal ions). For example, the {Fe-CN-Co} distances in the preferential face of Cs^+ average 5.02 Å, while in the opposite one the distances are slightly shorter, averaging 4.94 Å. The larger {Fe-CN-Co} distance is caused by the presence of the Co^{II}_{HS} ion in such face and is consistent with the slight displacement of the Cs^+ toward the face that bears the partial local negative charge of the {Co^{II}(Tp)$(\underline{N}C)_3$}$^{0.5-}$. The structural analysis of the **A⊂{Fe_4-Co_4}** cubes also reveal the presence of short contacts (shown in Figure 1), between the alkali ion and the cyanide bridges.

Such an interaction, noted A^+-π_{CN}, has already been discussed for FeCo PBAs.[20] It could be described as an interaction between the alkali cation, a Lewis acid, and the π-system of the cyanide, which can be seen as a Lewis base (note that this interaction is considered when the distance between A···C and A···N is below the sum of the van der Waals radii). Table 1 gives an overview of structural data that are relevant for the analysis

Table 1. Selected structural data related to the interaction between the cation and the cage in phase 1

	K^+	Rb^+	Cs^+
r_{ion} (Å)	1.52	1.64	1.81
VdW V (Å^3)	14.66	18.43	24.76
A···Co^{II} (Å)$^{(§)}$	3.91(6)	4.23(3)	4.31(3)
Number of A-π_{CN} interactions	3	5	12
A-C_{CN} short contacts range (Å)	3.2-3.4	3.5-3.4	3.43-3.66
Distortion $\sum$ (*deg*) $Co^{II\,(\#)}$	27	22	20

(§) shortest value (#) value on the most distorted Co site

of the cation-cage interaction in phase 1. In the case of **K⊂{Fe$_4$-Co$_4$}**, the close proximity of K^+ to the Co^{II}_{HS} corner (Table 1) results in significantly short K···C and K···N distances for the three π-cyanide systems linked to the Co^{II} ion. The K^+ ion is therefore only in interaction with these three cyanide bridges. In contrast, for **Cs⊂{Fe$_4$-Co$_4$}**, the Cs···C/N distances vary between 3.43-3.58 Å in the closest face but are similar to those in the opposite face (3.50-3.66 Å). Overall, the Cs^+ ion, whose size fits well the cavity, interacts with all twelve cyanide-π systems. In **Rb⊂{Fe$_4$-Co$_4$}**, the Rb^+ is situated marginally off-center at 4.23(2) Å from the Co^{II}_{HS} ion. The average Co-N distance of the Co ion located near the Rb^+ is *ca*. 1.99(1) Å whereas the average distance of the other Co-N distance is 1.92(1) Å. Slightly more decentered than the Cs^+, but not as close to the {Co(Tp)(N̲C)$_3$} edges as the K^+, the Rb^+ is in interaction with five cyanide bridges. Importantly the close interaction of the alkali ions with the $\{Co^{II}(Tp)(\underline{N}C)_3\}^{0.5-}$ site is directly correlated to the local distortion on the Co^{II} coordination sphere. This is reflected in the values of $\sum$, that represent the sum of the deviations from 90° of the twelve pseudo-orthogonal N-Co-N angles of the Co coordination sphere (Table 1) and that increases from $\sum$(Cs) < $\sum$(Rb) < $\sum$(K). It should be underlined that structural analysis from XRD data underestimates the actual distortions of the molecule since the distances and angles are averaged due to the statistical distribution of the Co(II) ion. Alternatively, EPR spectroscopy can be used as a local probe to evaluate the Co(II) site distortion, which is reflected into the anisotropy of the EPR signal. As expected for octahedral HS Co(II) ion, typical axial spectra corresponding to an effective spin ½ are observed at low temperature for all cubes. For both crystal phases and in frozen solution (see ESI), the splitting, $g^{eff}_{\parallel}$-$g^{eff}_{\perp}$ that is related to the axial distortion, is higher for **K⊂{Fe$_4$-Co$_4$}** than for **Rb⊂{Fe$_4$-Co$_4$}** and **Cs⊂{Fe$_4$-Co$_4$}**. The enhanced distortion for the smaller alkali cations is thus also supported by EPR data. The analyses of the magnetic susceptibility data (details in ESI) are also fully coherent with these observations. In particular a clear correlation is established between the axial distortion parameter, Δ, and the structural distortion in the Co coordination sphere (see Table 2 and details in ESI). Note that the differences in the interaction of the alkali ion with the cyanide bridges is also detectable in the FT-IR spectra of the cubes, as it impacts their cyanide stretching bands (see ESI). Cyanide stretching vibrations are sensitive to their coordination environment and a small change in their electronic properties often leads to visible shifts.

Finally, it is interesting to compare the structural data of the **A⊂{Fe$^{II}_4$-Co$^{III}_3$Co^{II}}** cubes with those of the oxidized cubes, **A⊂{Fe$^{II}_4$-Co$^{III}_4$}$^+$**, where the only Co^{II}_{HS} ion is converted into Co^{III}_{LS}. This provides an idea about possible modifications in the interactions of A^+ with the cubic cage upon a redox state change. In fact, as shown in previous works on related systems, the structural reorganization induced by the ETCST, Fe^{II}_{LS}-CN-Co^{III}_{LS} ⇔ Fe^{III}_{LS}-CN-Co^{II}_{HS}, mainly takes place on the Co-coordination sphere (due to the attendant spin transition), while the $\{Fe^{III/II}(Tp)(CN)_3\}$ subunit undergoes only slight structural changes.[44,45,36] For example, the average Fe-C or Fe-N bond lengths changes upon oxidation/reduction are in the range of *ca*. 0.02-0.04 Å. In the absence of structural data of the photo-induced forms, the oxidized cubes thus provide good models to estimate the structural reorganization that can occur upon an electronic state switching. In this work, we were able to isolate **K⊂{Fe$^{II}_4$-Co$^{III}_4$}$^+$** as a perchlorate salt (details in ESI). In this cube all of the four cobalt ions are in a low-spin diamagnetic state. In contrast to the paramagnetic cube, the K^+ ion is located in the center of the cavity, on the gravity center of the cube, and does not show short contacts with any of the cyanide ligands. These structural data clearly indicate that the K^+ cation can move inside the cavity and modify its interactions with the cyanide cage as the cube undergoes a change in its electronic state. Such structural change is also accompanied by a modification of the distortion of the cubic cage, as the coordination sphere of the Co^{III}_{LS} ion is significantly less distorted ($\sum \sim 9°$) than that of the Co^{II}_{HS} (see ESI). These structural changes are expected to be much less prominent for the larger Cs^+ ion, that already almost occupies the cage's center with dissymmetric distribution of the charges at the corner (*vide supra*), and established short contact with all twelve cyanide bridges.

Table 2. Distortion in the A⊂{Fe$_4$-Co$_4$} core measured by different observables in phase 1 (details in text).

	K^+	Rb^+	Cs^+
$g^{eff}_{\parallel}$-$g^{eff}_{\perp}$ (in CH_3CN solution)	6.05 (6.22)	5.84 (5.97)	5.62 (5.67)
Distortion Δ (cm^{-1})	-994	-759	-710

Concerning the intermolecular interactions, the neutral cubic units are isolated from each other in both phases and no short contact are detected between their organic shells. The shortest Fe···Fe, Fe···Co and Co···Co distances between neighboring cubes are *ca*. 10, 11.5 and 11.5 Å in the phase 1, and 11.8 Å in the phase 2 (where Fe and Co are indiscernible). The large distances between the cobalt metal ions are coherent with the observed EPR spectra that are typical of isolated octahedral Co^{II} complexes. The supramolecular organization of the cube and solvent CH_3CN molecules in the phase 1 is detailed in ESI.

To summarize all the structural analyses, the amount and nature of A^+-π_{CN} interactions in the **A⊂{Fe$_4$-Co$_4$}** cubes depend on the nature of the inserted alkali ion as well as on the redox state of the cages. Changes in the electronic state of the

cage can induce a motion of the inserted alkali ion, significant changes in the Co coordination sphere, and distortions in the cubic skeleton. While those changes are significant for the small K^+ and result in a stronger distortion of the cube, they are notably less important for the large Cs^+ alkali ion.

Photomagnetic Properties in the Solid-State

The photomagnetic responses were first investigated in the solid state for all three cubes **A⊂{Fe$_4$-Co$_4$}** in phase 1 and phase 2. To obtain comparable data, the six samples were studied following the same procedure of irradiating 0.3 mg of the samples at 20 K and with a 808 nm light source, which was proved to be very efficient in such cubic systems (power *ca*. 6 mW/cm^2).[39]

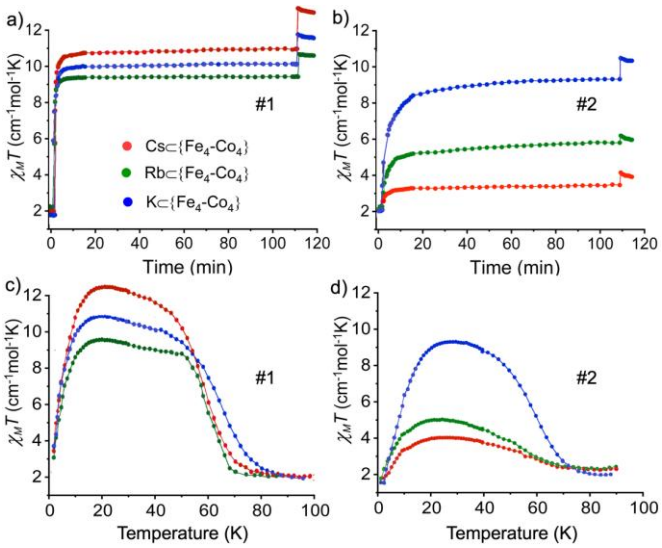

Figure 2. $\chi_M T$ *versus* time curves obtained upon irradiation at 20 K with 808 nm (5mW/cm^2) of A⊂{Fe$_4$-Co$_4$} in phase 1 a) and in phase 2 b). $\chi_M T$ *versus T* curves of the photo-induced metastable state measured upon heating at 0.4 K/min in phase 1 c) and in phase 2 d).

Figures 2 a) and 2 b) show the $\chi_M T$ value *versus* time for these six materials (χ_M is the molar magnetic susceptibility per cubic unit). This also implies that only three {Fe^{II}_{LS}-CN-Co^{III}_{LS}} diamagnetic pairs are able to switch into {Fe^{III}_{LS}-CN-Co^{II}_{HS}} paramagnetic ones. Taking into account the relative error on the measurements, we can consider that the photomagnetic responses in phase 1 are similar for all three **A⊂{Fe$_4$-Co$_4$}** cubes, regardless of the nature of A. For each compound, a rapid increase of the $\chi_M T$ value associated with the photo-induced conversion of diamagnetic pairs into paramagnetic ones is observed. A saturation value close to 10.5, 11.8 and 12.8 cm^3 mol^{-1} K for the Rb-, K- and Cs-cube respectively, is obtained within less than 10 minutes. The maximum $\chi_M T$ values, indicate a quantitative conversion that could roughly correspond to the switching of three Fe-Co pairs. In contrast, the photo-induced electron transfer in phase 2 is slower, and more importantly, the saturation values are lower and are quite different for the three cubes. They reach approximately 3.8, 5.8 and 10.2 cm^3 mol^{-1} K for the Cs-, Rb- and K-cubes, respectively. In summary, depending on the crystal phase, the inserted alkali ion seems to have different effects on the efficiency of the photomagnetic effect. Two results need to be underlined: (i) in contrast with PBAs, which do not show photomagnetic effect if Cs^+ ions occupy all interstitial sites, the presence of the large Cs^+ ions in the {Fe$_4$-Co$_4$} cubic cavities does not prevent a full conversion of the diamagnetic pairs into paramagnetic ones. Actually, in FeCo PBAs, the occupancy of all cavities by Cs^+ ions was shown to confer a stiffness to the coordination network, preventing the ETCST and the associated structural reorganization (the volume increase is accompanied by the lengthening of Co-N distances). In contrast, in the molecular model complexes, the switchable cubic units are not tightly bound to each other by coordination bonds and one can assume that the crystal lattice can absorb the structural changes. (ii) The very same **A⊂{Fe$_4$-Co$_4$}** cubic molecule can show very different photo-conversion rate depending on weak solid-state effects. This is reminiscent of previous studies that already showed the impacts of the presence of solvent molecules,[46–48] or different non-coordination anions[49] and more generally the crystal packing,[50,51] on the photo-induced ETCST. Only in few studies, clear correlation were established on the role of intermolecular interactions (H-bonding, π stacking or structural constraints) on the thermally- or photo-induced ETCST.[35–37] In the present case, the limited quality of the structural data in the phase 2 makes difficult establishing such correlation.

Once saturation was reached, the relaxation of the magnetization (Figures 2c and 2d) has been investigated by measuring the $\chi_M T$ value upon temperature increase under the same conditions (0.4 Kmin^{-1}). For all compounds, the curves roughly show three areas. At low temperature, typically below 20 K, there is a significant decrease of the $\chi_M T$ value upon cooling. This is ascribed to the occurrence of intermolecular antiferromagnetic interaction in the photoinduced metastable state. Above *ca*. 40 K, the decrease of the $\chi_M T$ value upon heating is due to the thermally activated relaxation to the diamagnetic state. It is more difficult to unambiguously analyze the magnetic behavior observed in the range the range between 20-40 K. The slight increase of the $\chi_M T$ value observed upon cooling could be the signature of weak intramolecular ferromagnetic interaction in the photoinduced state.[52]Actually, weak ferromagnetic interactions were observed in the Fe-CN-Co moieties.[53] However, the slope between 20-40 K could also be ascribed to the effect of a first relaxation regime, for example of quantum origin, operating before the thermally activated one.[54] An in-depth analysis of the relaxation actually suggests the occurrence of two relaxation regimes (see ESI). The relaxation temperatures, T_{Relax}, were obtained as the inflexion point of the $\chi_M T$ decrease above 40 K (*i.e.* as the minimum of the $\chi_M T$ *vs T* derivative). In phase 1, the T_{Relax} of the K-cube (67 K) is notably higher than that of Rb- and Cs-cube, which are closer to each other (respectively 59 and 57 K). In phase 2, T_{relax} are closer but follow the same order, from 57 K for K to 54 K for Cs. This trend is similar to that observed for PBAs and suggests a better stabilization of the metastable photo-induced state for the K-cube.

Photomagnetic Properties in Frozen Solutions

To get rid of the effects of intermolecular interactions that are present in crystalline materials, and to get a better insight on the role of the alkali ion, we took profit of the solubility and stability (verified by solution NMR and EPR, see ESI) of the cubic complexes to probe their behavior in frozen solution. The photomagnetic response of the three cubic molecules were thus investigated upon irradiation at 808 nm at 15 K in both

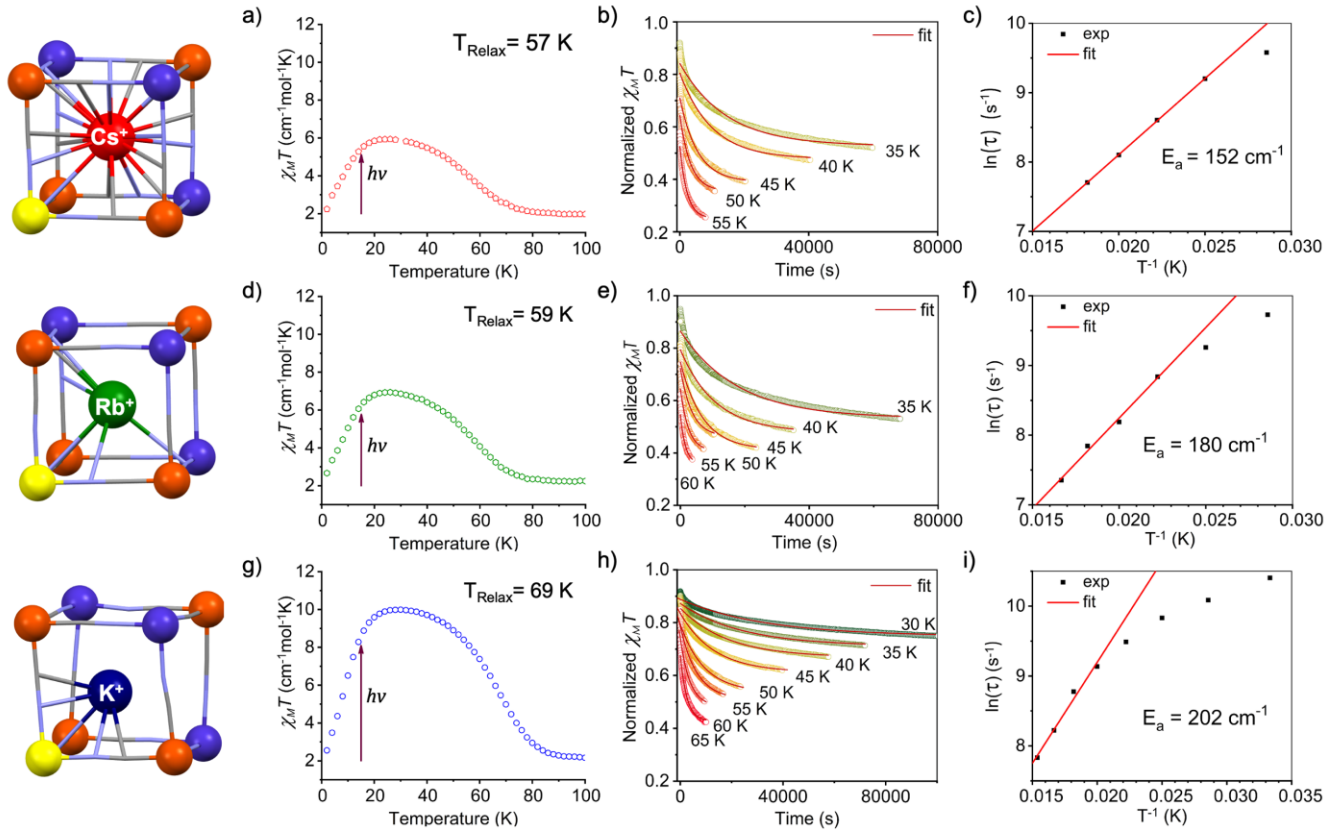

Figure 3. Magnetic measurements performed on a 5 mM CH_3CN solution of **A⊂{Fe$_4$-Co$_4$}**: $\chi_M T$ curves of the photo-induced metastable state measured upon heating at 0.4 Kmin^{-1} for A = Cs (a), Rb (d) and K (g). The arrows represent the increase of magnetization under irradiation at 15 K (808 nm light source, 5mW/cm^2). The relaxation temperature is defined as the inflexion point of the decreasing curves (see ESI); Isothermal relaxation curves measured after magnetic saturation upon light irradiation at 15 K for A = Cs (b), Rb (e) and K (h). Arrhenius-plot and resulting energy barrier E_a obtained by fitting the data in the high-temperature range A = Cs (c), Rb (f) and K (i). The first, second and third line gather the data of the Cs, Rb and K cube respectively.

acetonitrile solution, as well as in dichloromethane solutions for comparison (experimental details are given in ESI). Figures 3 (a, d and g) shows the photo-conversion of the dia- to the paramagnetic state (indicated by an arrow in the $\chi_M T$ *versus* T curves) and the thermal relaxation of the metastable state ($\chi_M T$ *versus* T curves after photo-irradiation) of **A⊂{Fe$_4$-Co$_4$}** in a 5 mM acetonitrile solution. In all these experiments, 45 µL of the complex solutions were introduced in the SQUID near liquid nitrogen temperature to immediately freeze the solutions (no precipitation was observed at these concentrations and low temperature in NMR tubes). At 15 K, all cubes exhibit a paramagnetic signal corresponding to the presence of one paramagnetic Co^{II}_{HS} ion. Upon light irradiation the $\chi_M T$ values increase, which accounts for the photo-induced electron transfer. In contrast with the solid-state experiments, the increase of $\chi_M T$ is more gradual and saturation values are not fully reached after 40 minutes. This is likely due to the absence of cooperative effect in frozen solution, where molecules are isolated from each other. Among the complexes, the **K⊂{Fe$_4$-Co$_4$}** cube shows the highest photo-conversion rate with a saturation value at *ca*. 8.3 cm^{3}mol^{-1}K in both solvents. The **Rb⊂{Fe$_4$-Co$_4$}** and **Cs⊂{Fe$_4$-Co$_4$}** only reach $\chi_M T$ values of 6.0 (4.8) cm^{3}mol^{-1}K for the Rb- and 5.5 (3.1) cm^{3}mol^{-1}K for the Cs-cube in acetonitrile (dichloromethane). Note, that the trend of efficiency is the same in both solvents.

The thermal relaxation of the photoinduced metastable state was also probed in both solvents. Once magnetic saturation was achieved upon irradiation, the laser was switched off and the sample slowly heated at 0.4 K/min from 2-140 K. The relaxation temperatures obtained as described above are shown in Figure 3 (a, d, g) and Table S9 (ESI). They indicate that the stability of the photoinduced state decreases with the size of the alkali ion from $Cs^+ < Rb^+ < K^+$ in a similar way as that observed in PBAs or in phase 1 (see above). However, slight differences are observed depending on the solvent. While the relaxation temperatures spread over 12 K in acetonitrile, T_{relax} values are separated by *ca*. 6 K in dichloromethane. Another difference lies in the form of the $\chi_M T$ *versus* T curves: while the $\chi_M T$ decrease is smooth and round in acetonitrile, the curve in dichloromethane (ESI) seems to show distinct relaxation regimes depending on the temperature range. Fitting these curves led to acceptable fits only for polynomials of degree n $\geq$ 5 so that two inflection points can be observed during relaxation that give rise to a second set of T_{Relax} noted in brackets (Table S9). In order to get quantitative data on the relaxation process, we conducted isothermal relaxation measurements in acetonitrile at different temperatures in order to access the energy barrier, E_a, between the ground and metastable state (Scheme 1). The results are shown in Figure 3 (b, e and h), where the normalized magnetization, M_t, is given against time (see details in ESI). As expected for isolated molecules, the isothermal relaxation curves can be fitted using a single exponential law: [55,56]

$$M_t = M_0\, e^{-k_{HL}(T)t} + y_0 = e^{-\frac{1}{\tau(T)}t} + y_0 \quad (1)$$

where τ(T) is the lifetime of the photoinduced metastable state and k_{HL}(T) is the rate constant of the first degree of the relaxation process. Due to the paramagnetic Co^{II}_{HS} ion present in the ground state, the magnetization does not tend to zero and it is therefore necessary to introduce a y-axis section y_o in the fitting function. This parameter slightly depends on the temperature as the magnetization of octahedral Co^{II}_{HS} complex slightly increases with rising temperature because of the effect of the spin-orbit coupling.[57] The fits of the measured relaxation curves are depicted in Figure 3 (b, e and h) as red lines and the thereof extracted values for τ (T) are listed in ESI. The ln(τ(T)) *versus* T^{-1} plots (Figure 3, c, f and i) show two distinct regions. At high temperature (T > 50 K), the dependence of ln(τ(T)) is linear, following the expected Arrhenius law. The E_a values can simply be extracted as the slope (see below). At lower temperature, beneath threshold temperatures of approximately 50, 45 and 40 K for the K-, Rb- and Cs- cubes, the curves depart from linearity and tend to flatten as T^1 increases. In other words, the relaxation tends to become temperature-independent. Such behaviors are commonly observed in spin-crossover complexes, in the relaxation process of photo-induced metastable high-spin state.[58–60] As for the bulk samples, they are ascribed to the changeover from a thermally activated relaxation regime to a quantum-induced relaxation regime at low temperature. Thus, we assume the situation is similar for our ETCST systems. As expected from the comparison of the life-times and the relaxation temperatures, the activation energy of **K⊂{Fe$_4$-Co$_4$}** is with (204 ± 6) cm^{-1} the highest one. The activation energy of **Rb⊂{Fe$_4$-Co$_4$}** is with (180 ± 11) cm^{-1} about 24 cm^{-1} lower, but **Cs⊂{Fe$_4$-Co$_4$}** has with (152 ± 2) cm^{-1} the lowest energy barrier. Note that this trend also holds when taking into consideration the calculated error marge. Up to now, the only photomagnetic molecule showing ETCST where this energy barrier has been reported is a **{Fe^{III}_4-Co_4^{II}}$^{4+}$** empty cube reported in 2008 by *Li et al.*[61] With a relaxation temperature more than twice as high (180 K at a scan rate of 0.3 $Kmin^{-1}$) as compared to the present **A⊂{Fe$_4$-Co$_4$}** cubes, the calculated energy barrier amounts to *ca.* 3096 cm^{-1}, which is one magnitude higher. This elevated energy barrier leads to a lifetime τ ≈ 10 years of the photoexcited state at 120 K. A large energy barrier of *ca.* 2161±42 cm^{-1} (T_{Relax} = 132 K) was also obtained for the three dimensional PBA, $Na_{0.32}Co[Fe(CN)_6]_{0.74}\cdot 3.4\ H_2O$, that revealed a lifetime τ ≈ 33 h at 120 K.[62–64] As these values were obtained in solid-state measurements where the energy barrier is influenced by the lattice matrix and intermolecular interactions, we also conducted relaxation studies on crystals of **K⊂{Fe$_4$-Co$_4$}** in phase 1 to evaluate the influence of the solid-state interactions on the relaxation. Like in frozen solution, the isothermal relaxation curves (see ESI) can be fitted by a single exponential so that we can conclude that this crystal phase is showing low to almost no cooperativity.[65] This is coherent with the crystal structure data that do not reveal any significant intermolecular interactions between the cubic units. Like in frozen solution, the analysis of the relaxation rates (Arrhenius plot shown in ESI) points to a changeover from a relaxation regime governed by tunnelling to a thermally activated regime above 50 K. The measured lifetimes τ(T) (details in ESI) are only slightly higher than for the compound in frozen solution and the resulting energy barrier, E_a = 350 cm^{-1} is higher but of the same order as the one measured in solution. The energy barriers of the presented **A⊂{Fe$_4$-Co$_4$}** cubes are thus intrinsic properties of the molecules. It is difficult to establish the origin of the high barrier observed in the previously reported **{Fe$_4$-Co$_4$}** cube taking into account the limited number of relaxation studies on FeCo charge transfer system. The previously proposed correlation between the high energy barrier and the higher nuclearity (in comparison to tetrametallic square or bimetallic pair complexes)[66] is uncertain when considering the present results. The measured energy barriers in this work are in fact much more similar to those found in some Fe(II) spin-crossover (SCO) complexes and to the HS to LS relaxation measured on diluted systems with comparable relaxation temperatures.[67,68,69,70]

Overall, the relaxation studies confirm that the nature of the intercalated cation plays a significant role on the photomagnetic effect. The smaller the cation, the higher the relaxation barrier, E_a and the relaxation temperature, T_{Relax}. In other words, the photoinduced metastable state is stabilized by the presence of the smaller potassium cation, similarly to the trend reported for Na, Rb and Cs PBAs.[20] A possible origin of this observation could be found in a stronger structural reorganization when passing from the ground to the metastable state. This corresponds to a horizontal displacement in the scheme 1 that depict the Gibbs energy of dia- and paramagnetic states *versus* reaction coordinate. Alternatively, Bleuzen *et al.* postulated that small cations would stabilize the Co(II) redox state and thus the $Fe^{III}_{LS}Co^{II}_{HS}$ metastable state. This corresponds to a vertical displacement in the scheme 1. The investigation of the $Fe^{II/III}$ and $Co^{II/III}$ redox processes in the three cubes can give some indication on the influences of the alkali ion on the stabilization of the Co^{II} redox state, and on the structural reorganization that accompanies the Co^{II}_{HS} ⇔ Co^{III}_{LS} electronic state change. In the following part, we thus take profit of the cube's stability in solution to investigate their redox behaviour by cyclic voltammetry.

Scheme 1. Horizontal and Vertical Displacements: Sketch of $Fe^{II}_{LS}Co^{III}_{LS}$ and $Fe^{III}_{LS}Co^{II}_{HS}$ potential wells as a function of d(Co-N) and possible displacements.

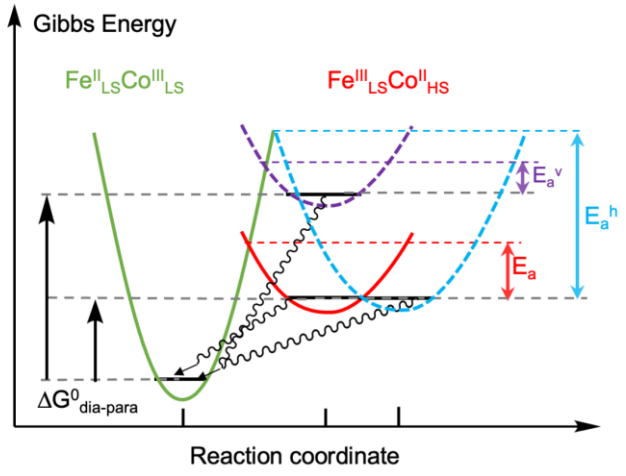

Variable Temperature Cyclic Voltammetry

Cyclic voltammetry studies were performed in acetonitrile solutions containing 0.1 M of NBu_4PF_6 as supporting electrolyte at various temperatures. Figure 4 shows a typical cyclic voltammogram of **Rb⊂{Fe$_4$-Co$_4$}**. As previously described for

Cs⊂{Fe$_4$-Co$_4$}, eight oxidation events are expected. Four of them, which are chemically and electrochemically reversible events, are observed at high potential, between approx. 0.9 and 1.5 V versus SCE. They correspond to the successive oxidation and reduction of the $Fe^{II/III}$ ions. The remaining four located at lower potentials, between -1.2 and 0.6 V, show a large splitting between the oxidation and reduction waves, which is typical of chemically reversible but electrochemically irreversible redox processes, and they are ascribed to the $Co^{II/III}$ couples. The open circuit potential (OCP) is located around 0.05 V, below the last Co^{II}/Co^{III} oxidation process, confirming the presence of one Co^{II} and three Co^{III} ions in the cubes (see ESI). In the following, we first discuss the $E^0(M^{II/III})$ redox potentials, which are linked to the thermodynamic properties of the systems, and that are related to the vertical displacement as depicted above. Then we discuss the splitting between the oxidation and reduction potentials of the $Co^{II/III}$ ions, $DE_p = E_{ox}(Co^{II}) - E_{red}(Co^{III})$, which is linked to electron transfer kinetic properties and the associated structural reorganization, and thus related to the horizontal displacement of the reaction coordinate in Scheme 1.

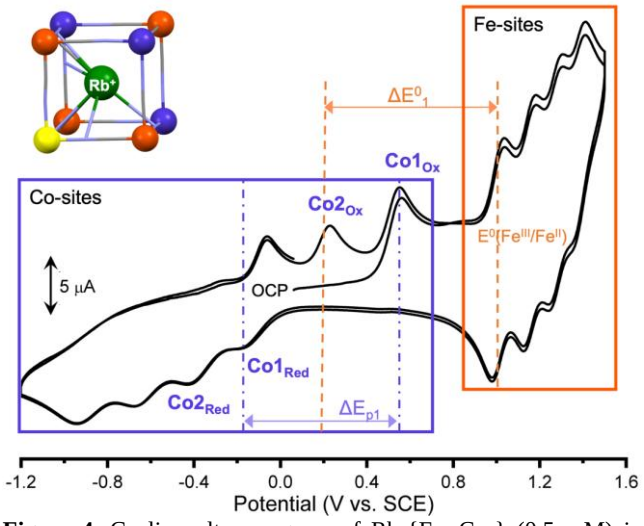

Figure 4. Cyclic voltammogram of Rb-{Fe$_4$-Co$_4$} (0.5 mM) in CH_3CN with 0.1 M $^tBu_4PF_6$ at 288 K using a glassy carbon WE (3 mm diameter) and Pt-wire CE.

As in ETCST process, the electron transfer occurs between the Fe and Co ions, we took as reference the redox potential of the Fe and we more specifically compare the differences $\Delta E^0_1 = E^0(Fe^{III}/Fe^{II})_1 - E^0(Co^{III}/Co^{II})_1$ and $\Delta E^0_2 = E^0(Fe^{III}/Fe^{II})_1 - E^0(Co^{III}/Co^{II})_2$ of the first switching pairs. While the $E^0(Fe^{III}/Fe^{II})$ are almost temperature independent, $E^0(Co^{III}/Co^{II})$ are sensitive to temperature changes. This is correlated to the important entropy change associated with this redox process. Actually, an increase of entropy is expected upon conversion of the Co^{III}_{LS} (S = 0) into the Co^{II}_{HS} state (S = 3/2). On the one hand, the spin multiplicity increases. On the other hand, the weaker bond strength in the Co^{II}_{HS}-ligand bond (correlated to the population of antibonding e_g* orbitals) is associated with a higher density of vibrational states and a higher vibrational entropy contribution than in the Co^{III}_{LS} state. This entropy variation explains both the positive shift the Co redox potentials as the temperature increases, and the stabilization of the $Fe^{III}_{LS}Co^{II}_{HS}$ paramagnetic state over the $Fe^{II}_{LS}Co^{III}_{LS}$ diamagnetic one at high temperature in complexes showing thermally induced ETCST. It is worth noticing that the temperature dependence is stronger for **K⊂{Fe$_4$-Co$_4$}** as shown in ESI and in Figures 5a and 5b where we plot respectively ΔE^0_1 and ΔE^0_2 for the three cubes. Both ΔE^0_1 and ΔE^0_2 are larger in Cs- and Rb- than in the K-cube at room temperature, however this difference strongly decreases upon cooling. The temperature-dependence of the potentials even suggests an inversion at lower temperatures. Two important points should be underlined from these data. First, the strong T-dependence indicates that entropic effects are playing a key role in Scheme 1, in particular for **K⊂{Fe$_4$-Co$_4$}**. The larger entropy variation for the K cube could well be related to the higher "mobility" of the inserted K^+ cation and the larger distortions as shown by our XRD, EPR and magnetic data. Secondly, a higher $\Delta E^0_{1,2}$ value for **K⊂{Fe$_4$-Co$_4$}** at low temperature would suggest that the diamagnetic $Fe^{II}Co^{III}$ pair are better stabilized in that cube than in the Rb and Cs ones. In other words, the Co(II) redox state would be better stabilized with the larger alkali ions. This result does not support the hypothesis proposed by Bleuzen *et al*., which was used to explain the trend: $E_a(Cs) < E_a(Rb) < E_a(K)$. Here, it is worth reminding that this first hypothesis was drawn taking into account the energy gap between the diamagnetic and paramagnetic states (vertical displacement) but neglecting any possible impact of structural distortion.

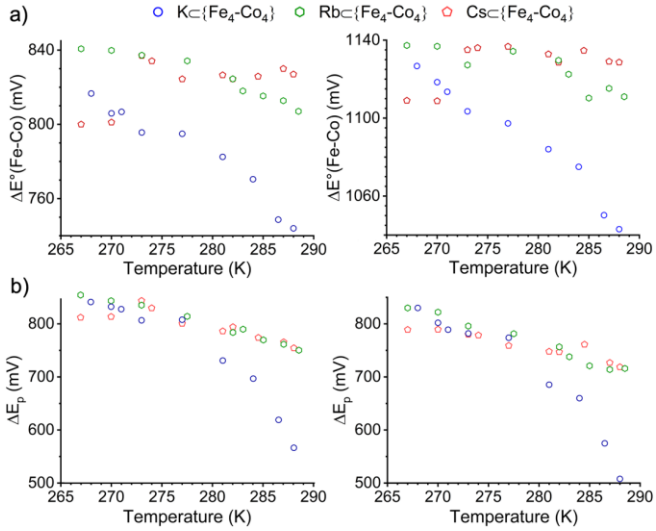

Figure 5. (a) Peak-peak potential difference ΔE°(Fe-Co) = E°(Fe)- E°(Co) of Co1 (left) and Co2 (right) as a function of the temperature. (b) Peak-peak potential difference $\Delta E_p = E_{ox}(Co^{II}) - E_{red}(Co^{III})$ of Co1 (left) and Co2 (right) as a function of the temperature.

Actually, the structural changes also play a key role in the electron transfer kinetics as depicted in the Marcus-Hush theory of electron transfer.[71,72] Here, the slow kinetics of electron transfer is reflected through a very large separation ΔE_p between the oxidation and reduction peak potentials of the Co entities and reveals important differences between the bond lengths and angles of the reduced and oxidized forms. This behaviour was also observed for example in the related complex $[Co^{II/III}(Tp)_2]$, where ΔE_p amounts to *ca*. 200 mV, which can be correlated to the energy barrier associated with the spin change.[73–75] In the **A⊂{Fe$_4$-Co$_4$}** cubes, the shifts are much larger and reach *ca*. 840 mV at 267 K. The very important ΔE_p obtained here suggest that in addition to the reorganization energy of the cobalt close coordination sphere (Co-N distances

and distortion of the coordination sphere), the cage distortions and movements of the alkali cation (and interactions with the π_{CN} bonds) systems should also be taken into account as demonstrated by the solid-state structural studies (Figure 1). As temperature decreases, it is noticeable that ΔE_p for **K⊂{Fe$_4$-Co$_4$}** vary strongly to become comparable to those obtained for the two other systems, and would also become larger at lower temperatures, in agreement with a stronger structural reorganization, as suggested by the XRD analyses (*vide supra*). We remind however here that electrochemical kinetic data only partly reflect the behavior in photomagnetic experiments. For example, one of the difference stems from the solvent reorganization, that we expect to be more important in electrochemistry since a net charge appears whereas there is none in photomagnetism. We do not however expect any important difference between the A-cubes implied by the solvent. Advanced cyclic voltammetry measurements, at very-high scan rates and on a broader temperature range could bring in the future more insight on both kinetic and thermodynamic of the ETCST involved in the $Co^{II}_{HS} \Leftrightarrow Co^{III}_{LS}$ conversion. Nonetheless, at this stage this seminal electrochemical study is consistent with the assumption that the structural reorganization may contribute to the stabilization of the metastable state, but a stabilization of the Co(II) redox state by small alkali cations remains to demonstrate.

DISCUSSION

The confrontation of structural, spectroscopic and electrochemical studies on this **A⊂{Fe$_4$-Co$_4$}** cubic models and their comparison with previous studies on PBAs allows enlightening the possible respective role of the structural rearrangement and the relative stabilization of the paramagnetic $Fe^{III}_{LS}Co^{II}_{HS}$ metastable state. A ***horizontal displacement*** (depicted in light blue in the scheme 1) corresponding to geometrical changes between the initial diamagnetic state and the paramagnetic one leads to an increase in E_a. To take into account the effect of the nature of the alkali ion, this parameter cannot be restricted to the variation in the Co-N bond lengths that are similar for all cubes, but it should include the distortion in the Co coordination sphere. A clear correlation can thus be drawn between the above discussed structural (and EPR) data and the stability of the metastable states observed in the **A⊂{Fe$_4$-Co$_4$}** cubes. We suggest that the higher differences in the Co coordination sphere geometry between Co^{II}_{HS} and Co^{III}_{LS} centers in the K-cube as compared to the Rb- and Cs-cubes is responsible, at least partially, for a larger E_a. In fact, from the above structural data, one can expect that an electron transfer in the Cs-cube would induce a moderate structural distortion on the Co^{II} center as the structural study show that the Cs^+ interacts with all twelve cyanide bridges, which in turn restrains the distortion of the Co^{II}_{HS} coordination sphere compared to that observed in the K cube. A similar hypothesis has been made for Fe^{II} SCO complexes by Létard *et coll.* A simple linear correlation between the Fe-N bond length variation and the stability of the photoinduced state of the widely studied Fe-SCO complexes was shown to be unsatisfactory.[76,77] The distortion of the coordination sphere emerged as a key parameter.[78–80] In fact, by screening series of Fe^{II} SCO complexes Létard *et coll.* clearly established that the trigonal distortion of the coordination polyhedron varies linearly with T_{relax} (or T_{LIESST}), when complexes exhibit similar bond lengths and crystal packings.[81]

Beyond the changes in the distortion of the coordination sphere, other structural modifications could accompany the ETCST: a motion of the alkali ion induced by a modification of the local charges (and consequent changes in the $A^{\cdots}\pi_{CN}$ interactions), changes in the distortion of the cubic framework, *etc*. At this stage it is interesting to note that studies on photo-active $Na_2Co_4[Fe(CN)_6]_{3.3}\cdot 14H_2O$ PBAs actually showed that the Na^+ undergoes a motion upon photo-induced electron transfer.[82] Further evidence of such motions have been found for the PBA of formula $Cs_{0.7}Co_4[Fe(CN)_6]_{2.9}\cdot 16H_2O$. At first glance, the remarkable photo-efficiency of this Cs-based PBA and its relatively high relaxation temperature could seem contradictory with our findings. However, in that case, the PBA material shows vacancies: on average, the Cs^+ ion is located in a beheaded $\{Fe_4Co_3[]_1\}$ cubic unit ([] represents a $\{Fe(CN)_6\}$ vacancy). XAS results showed that in that case the Cs^+ ion moves from the center of the cube toward the vacancies, upon redox state change.[22] This contrasts with the situation observed on our cubic molecular models where the Cs^+ is trapped in the center of the closed cubic cavity.

The other factor that was previously considered to justify the differences in T_{relax} between PBA containing different alkali ions is the influence of the cation on the energy difference $\Delta G_{dia\text{-}para}$ (that we can assimilate to $\Delta H_{dia\text{-}para}$ at T = 0 K). This corresponds to a ***vertical displacement*** of the potential well of the metastable state (violet curve in the Scheme 1). A stabilization of the metastable state through a decrease of $\Delta H_{dia\text{-}para}$ leads to a higher energy barrier, E_a. A decrease of $\Delta H_{dia\text{-}para}$ is also expected to lead to a decrease of the transition temperature $T_{1/2}$ associated with the thermally induced transition. Actually $\Delta H_{dia\text{-}para}$ represents the enthalpy difference that needs to be counterbalanced by the entropy term $T\Delta S_{dia\text{-}para}$ to allow the thermally induced transition. Indeed, an inverse relationship was established in related SCO complexes between T_{LIESST} (analogous to T_{relax}) and $T_{1/2}$.[83] Such relationship was similarly observed by Bleuzen *et coll.* in the series of PBAs: $A_2Co_4[Fe(CN)_6]_{3.3}\cdot 11H_2O$ (A = Na, Rb, Cs).[20] This observation lead them to suggest that the smaller alkali cations (here the K^+) would stabilize the paramagnetic metastable state. The origin of this stabilization would be the stronger interaction between the small alkali ion, (that are stronger Lewis acids) with the cyanide ligand. This should decrease the donor ability of the N-cyanide atom, and consequently the ligand field on the cobalt ion. Ultimately, this should lead to a stabilization of the Co^{II} redox state and thus a stabilization of the Fe^{III}_{LS}-Co^{II}_{HS} paramagnetic state and a higher E_a in comparison to larger alkali ions. In the present case, the inverse trend between T_{Relax} and $T_{1/2}$ is also observed: the thermal ETCST in the solid state (phase 1) starts gradually between 300 – 400 K for **K⊂{Fe$_4$-Co$_4$}** and **Rb⊂{Fe$_4$-Co$_4$}**, and it is not yet observed for **Cs⊂{Fe$_4$-Co$_4$}** (see ESI). One could thus expect that the paramagnetic metastable state would be better stabilized for the K-cube. However, the clear distinct T-dependence of the redox potential demonstrates that entropy variation, $\Delta S_{dia\text{-}para}$, depend on the alkali ion. It is important underlying that the inverse trend proposed for SCO and PBA is correct only if the entropy variations are similar between the systems that are compared. The observed inverse trend can thus be misleading. Indeed, electrochemical measurements that showed a larger entropy variation in **K⊂{Fe$_4$-Co$_4$}** allow extrapolating that the Cs cube could be better stabilized at low temperature and would exhibit the higher *Ea*. The present experimental results on this spe-

cific family show the opposite, and thus suggest that the higher activation energy barrier measured in the **K⊂{Fe$_4$-Co$_4$}** should rather arise from the higher structural reorganisation. At this stage, we believe there is a clear need for new studies on related systems and for advanced measurements that could help bringing more experimental information on the parameters stabilizing the metastable state. Advanced cyclic voltammetry measurements, at very-high scan rates and on a broader temperature range could bring in the future more insight on both kinetic and thermodynamic of the ETCST involved in the $Co^{II}_{HS} \Leftrightarrow Co^{III}_{LS}$ conversion.

CONCLUSION

The present study on **A⊂{Fe$_4$-Co$_4$}** molecular cubic models of photomagnetic FeCo PBAs allowed accessing accurate structural and electronic information that are not easily obtained in solid-state in the non-stoichiometric PBA inorganic polymers. The crystal structure analysis on single crystals reveals the distinct interactions of the alkali cations with the cage and their different mobility. In contrast with the large Cs^+ ion that fits well in the cubic cavity and establishes interaction with the twelve cyanide edges, the position of the smaller K^+ ion and its interaction with the cage can undergo strong changes as the electronic state of the cage changes. The nature of the alkali cation also impact the geometrical distortions that are observed in the HS-Co(II) ion. The solubility and stability of the cubic models has also allowed obtaining relaxation data in frozen solution, which allow limiting the influence of solid-state interactions on the relaxation process. A clear correlation emerges between the extent of the geometrical changes that can occur in the cubic cage upon a redox state change and the size of the inserted alkali cation. The larger geometrical changes observed for the K-cube well correlate with the larger activation energy that was deduced from frozen solution measurement. Similarly to SCO complexes, the distortion appears as a key factor that contributes to a stabilization of the metastable state. This can provide a guideline for designing systems in which relaxation temperature and metastable lifetime could be improved. In contrast, the CV data on the present family do not allow supporting the previously postulated stabilization of Co^{II}_{HS} state by small alkali ion. Further experimental data on other models, and if possible, in broader temperature range are needed to draw stronger conclusion. This study however allows underlying an important point: the redox potentials measured at room temperature that are sometimes used to compare FeCo charge transfer system should be taken with care. The clear T-dependence of redox potentials reveals that entropy variation may be different in closely related chemical systems.

EXPERIMENTAL SECTION

DC Magnetic susceptibility measurements were carried out using Quantum Design SQUID magnetometer. The measurement **on bulk materials** were obtained from freshly filtered samples (packed in a polyethylene bag), which were introduced in the SQUID at 200 K under helium flow and frozen before purging under vacuum. The measurements on bulk materials were performed in the temperature range 2 - 400 K under a magnetic field of 0.1 T (20 – 400 K) and 0.05 T (40 – 2 K). The magnetic susceptibility values were corrected from the diamagnetism of the molecular constituents and of the sample holder. Additional details on data treatments are given in ESI. For the photomagnetic and relaxation measurements on solid, approximately 0.4 mg of freshly filtered crystals (phase 1 and 2) were homogenously distributed on the adhesive face of a paper disk (diameter = 5 mm), which was mounted into a straw. The straw was then introduced in the SQUID at 110 K, before purging. The photomagnetic response was measured at 20 K using an 808 nm light source (*ca*. 10 mW/cm^2). Thermal relaxation curves ($\chi_M T$ *versus* T) were acquired by continuously heating the samples at 0.4 K min^{-1} from 2 to *ca*.150 K after reaching magnetic saturation due to light irradiation and then switching off the light source. Isothermal relaxation has been measured at different temperatures after irradiating the samples at 15 K.

Magnetic measurements **of frozen solutions** were carried out using 5 mM solution of the compounds in acetonitrile and dichloromethane. For this, 45µL of an acetonitrile and dichloromethane solution were introduced in a medicinal capsule, that was fixed between two glass rods (d = 3.5 mm, L = 6 cm) in a straw. The sample solution produces a diamagnetic signal, the gap between the glace rods, a paramagnetic one, and the overall signal is paramagnetic. This specific sample mounting allows the obtention of reliable magnetic data for the systems with very small sample size in a large diamagnetic media. The straw was introduced into the SQUID at 110 K to allow homogenous freezing of the solution without solid precipitation, and the SQUID magnetometer was purged once the solvent frozen. The photomagnetic response was measured at 15 K using an 808 nm light source (*ca*. 10 mW/cm^2). All magnetic data were corrected from the diamagnetic and paramagnetic contributions of the sample mounting. Thermal relaxation and isothermal relaxation curves were acquired in the same condition as for the bulk samples.

Cyclic Voltammetry

Cyclic voltammograms at variable temperature were recorded in a standard electrochemical cell inserted in a refrigerating calibration bath and using a Metrohm PGSTAT 101 electrochemical analyser. The temperature was controlled by inserting a thermometer directly into the solution. Measurements were carried out on acetonitrile solutions of *ca*. 0.5 mM of **A⊂{Fe$_4$-Co$_4$}** and using 0.1 M NBu_4PF_6 salt as supporting electrolyte. A 3 mm glassy carbon electrode and a Pt-wire were used as the working- and counter electrode and the potential was measured against a SCE as a reference. N_2 flux was used to degas the solution prior to each measurement.

EPR

The EPR spectra of bulk samples and frozen dichloromethane solutions were measured at X-band (9.34 GHz) with a Bruker ER200 instrument equipped with a liquid helium cryostat from Oxford, Inc. The temperature was varied between 4 K and 80 K with various microwave powers (0.02 - 2mW), and with a modulation amplitude of 10 Gauss and a modulation frequency of 100 kHz. Details about the data analysis are given in ESI.

XRD

A single crystal of each compound was selected, mounted onto a cryoloop, and transferred in the cold nitrogen gas stream of an Oxford Cryostream. Intensity data were collected at 200K with a BRUKER Kappa-APEXII diffractometer with either Cu or Mo radiation. APEX 3 suite and SAINT program (BRUKER) were used to carry out data collection, unit-cell parameters refinement, integration and data reduction. SADABS was used for scaling and multi-scan absorption

corrections. In the Olex2 suite or in the WingX suite, the structures were solved with SHELXT-14 program and refined by full-matrix least-squares methods using SHELXL-14. CCDC 2157683-2157685 contain the supplementary crystallographic data for new structures in this paper. The data can be obtained free of charge from The Cambridge Crystallographic Data Centre via www.ccdc.cam.ac.uk/structures

ASSOCIATED CONTENT

Supporting Information contain additional experimental details and experimental data concerning: the syntheses and crystallization procedure, elemental analyses, FT-IR, NMR, UV-vis and EPR spectra, cyclic voltammetry, XRD data, DC and AC magnetic measurements and data treatment.

The Supporting Information is available free of charge on the ACS Publications website.

AUTHOR INFORMATION

*rodrigue.lescouezec@sorbonne-universite.fr

The manuscript was written through contributions of all authors. All authors have given approval to the final version of the manuscript. ‡These authors contributed equally.

ACKNOWLEDGMENT

The authors acknowledge the Centre National de la Recherche Scientifique (CNRS) and Sorbonne Université for their funding. The authors thank Geoffrey Gontard for his help in the treatment of the structural data.

REFERENCES

(1) *Spin-Crossover Materials: Properties and Applications*; Halcrow, M. A., Ed.; Wiley: Chichester, 2013.

(2) Meng, Y.-S.; Sato, O.; Liu, T. Manipulating Metal-to-Metal Charge Transfer for Materials with Switchable Functionality. *Angewandte Chemie International Edition* **2018**, *57* (38), 12216–12226. https://doi.org/10.1002/anie.201804557.

(3) Koo, Y.-S.; Galán-Mascarós, J. R. Spin Crossover Probes Confer Multistability to Organic Conducting Polymers. *Adv. Mater.* **2014**, *26* (39), 6785–6789. https://doi.org/10.1002/adma.201402579.

(4) Molnár, G.; Rat, S.; Salmon, L.; Nicolazzi, W.; Bousseksou, A. Spin Crossover Nanomaterials: From Fundamental Concepts to Devices. *Advanced Materials* **2018**, *30* (5), 1703862. https://doi.org/10.1002/adma.201703862.

(5) Holovchenko, A.; Dugay, J.; Giménez-Marqués, M.; Torres-Cavanillas, R.; Coronado, E.; van der Zant, H. S. J. Near Room-Temperature Memory Devices Based on Hybrid Spin-Crossover@SiO_2 Nanoparticles Coupled to Single-Layer Graphene Nanoelectrodes. *Advanced Materials* **2016**, *28* (33), 7228–7233. https://doi.org/10.1002/adma.201600890.

(6) Senthil Kumar, K.; Ruben, M. Emerging Trends in Spin Crossover (SCO) Based Functional Materials and Devices. *Coordination Chemistry Reviews* **2017**, *346*, 176–205. https://doi.org/10.1016/j.ccr.2017.03.024.

(7) Urdampilleta, M.; Ayela, C.; Ducrot, P.-H.; Rosario-Amorin, D.; Mondal, A.; Rouzières, M.; Dechambenoit, P.; Mathonière, C.; Mathieu, F.; Dufour, I.; Clérac, R. Molecule-Based Microelectromechanical Sensors. *Scientific Reports* **2018**, *8*(1), 8061. https://doi.org/10.1038/s41598-018-26076-2.

(8) Pierpont, C. G.; Buchanan, R. M. Transition Metal Complexes of O-Benzoquinone, o-Semiquinone, and Catecholate Ligands. *Coordination Chemistry Reviews* **1981**, *38* (1), 45–87. https://doi.org/10.1016/S0010-8545(00)80499-3.

(9) Aguilà, D.; Prado, Y.; Koumousi, E. S.; Mathonière, C.; Clérac, R. Switchable Fe/Co Prussian Blue Networks and Molecular Analogues. *Chemical Society Reviews* **2016**, *45* (1), 203–224. https://doi.org/10.1039/C5CS00321K.

(10) Hayami, S.; Holmes, S. M.; Halcrow, M. A. Spin-State Switches in Molecular Materials Chemistry. *J. Mater. Chem. C* **2015**, *3* (30), 7775–7778. https://doi.org/10.1039/C5TC90128F.

(11) Sato, O.; Iyoda, T.; Fujishima, A.; Hashimoto, K. Photoinduced Magnetization of a Cobalt-Iron Cyanide. *Science* **1996**, *272* (5262), 704–705. https://doi.org/10.1126/science.272.5262.704.

(12) Cammarata, M.; Zerdane, S.; Balducci, L.; Azzolina, G.; Mazerat, S.; Exertier, C.; Trabuco, M.; Levantino, M.; Alonso-Mori, R.; Glownia, J. M.; Song, S.; Catala, L.; Mallah, T.; Matar, S. F.; Collet, E. Charge Transfer Driven by Ultrafast Spin Transition in a CoFe Prussian Blue Analogue. *Nat. Chem.* **2021**, *13* (1), 10–14. https://doi.org/10.1038/s41557-020-00597-8.

(13) Flambard, A.; Köhler, F. H.; Lescouëzec, R. Revisiting Prussian Blue Analogues with Solid-State MAS NMR Spectroscopy: Spin Density and Local Structure in [Cd3{Fe(CN)6}2]· 15 H2O. *Angewandte Chemie International Edition* **2009**, *48* (9), 1673–1676. https://doi.org/10.1002/anie.200805415.

(14) Flambard, A.; Köhler, F. H.; Lescouëzec, R.; Revel, B. Probing Spin Density and Local Structure in the Prussian Blue Analogues CsCd[Fe/Co(CN)6]· 0.5 H2O and Cd3[Fe/Co(CN)6]2· 15 H2O with Solid-State MAS NMR Spectroscopy. *Chemistry - A European Journal* **2011**, *17* (41), 11567–11575. https://doi.org/10.1002/chem.201100778.

(15) Simonov, A.; De Baerdemaeker, T.; Boström, H. L. B.; Ríos Gómez, M. L.; Gray, H. J.; Chernyshov, D.; Bosak, A.; Bürgi, H.-B.; Goodwin, A. L. Hidden Diversity of Vacancy Networks in Prussian Blue Analogues. *Nature* **2020**, *578* (7794), 256–260. https://doi.org/10.1038/s41586-020-1980-y.

(16) Champion, G.; Escax, V.; Cartier dit Moulin, C.; Bleuzen, A.; Villain, F.; Baudelet, F.; Dartyge, E.; Verdaguer, M. Photoinduced Ferrimagnetic Systems in Prussian Blue Analogues C^{I}_{x} Co_4 $[Fe(CN)_6]_y$ (C^{I} = Alkali Cation). 4. Characterization of the Ferrimagnetism of the Photoinduced Metastable State in $Rb_{1.8}$ Co_4 $[Fe(CN)_6]_{3.3}$ ·$13H_2O$ by K Edges X-Ray Magnetic Circular Dichroism. *Journal of the American Chemical Society* **2001**, *123* (50), 12544–12546. https://doi.org/10.1021/ja011297j.

(17) Bleuzen, A.; Lomenech, C.; Escax, V.; Villain, F.; Varret, F.; Cartier dit Moulin, C.; Verdaguer, M. Photoinduced Ferrimagnetic Systems in Prussian Blue Analogues C^{I}_{x} Co_4 $[Fe(CN)_6]_y$ (C^{I} = Alkali Cation). 1. Conditions to Observe the Phenomenon. *J. Am. Chem. Soc.* **2000**, *122* (28), 6648–6652. https://doi.org/10.1021/ja000348u.

(18) Cartier dit Moulin, C.; Villain, F.; Bleuzen, A.; Arrio, M.-A.; Sainctavit, P.; Lomenech, C.; Escax, V.; Baudelet, F.; Dartyge, E.; Gallet, J.-J.; Verdaguer, M. Photoinduced

Ferrimagnetic Systems in Prussian Blue Analogues C^{I}_{x} Co_4 $[Fe(CN)_6]_y$ (C^{I} = Alkali Cation). 2. X-Ray Absorption Spectroscopy of the Metastable State. *J. Am. Chem. Soc.* **2000**, *122* (28), 6653–6658. https://doi.org/10.1021/ja000349m.

(19) Escax, V.; Bleuzen, A.; Cartier dit Moulin, C.; Villain, F.; Goujon, A.; Varret, F.; Verdaguer, M. Photoinduced Ferrimagnetic Systems in Prussian Blue Analogues C^{I}_{x} Co_4 $[Fe(CN)_6]_y$ (C^{I} = Alkali Cation). 3. Control of the Photo- and Thermally Induced Electron Transfer by the $[Fe(CN)_6]$ Vacancies in Cesium Derivatives. *Journal of the American Chemical Society* **2001**, *123* (50), 12536–12543. https://doi.org/10.1021/ja011296r.

(20) Cafun, J.-D.; Champion, G.; Arrio, M.-A.; dit Moulin, C. C.; Bleuzen, A. Photomagnetic CoFe Prussian Blue Analogues: Role of the Cyanide Ions as Active Electron Transfer Bridges Modulated by Cyanide−Alkali Metal Ion Interactions. *Journal of the American Chemical Society* **2010**, *132* (33), 11552–11559. https://doi.org/10.1021/ja102660b.

(21) Trinh, L.; Zerdane, S.; Mazérat, S.; Dia, N.; Dragoe, D.; Herrero, C.; Rivière, E.; Catala, L.; Cammarata, M.; Collet, E.; Mallah, T. Photoswitchable 11 Nm CsCoFe Prussian Blue Analogue Nanocrystals with High Relaxation Temperature. *Inorg. Chem.* **2020**, *59* (18), 13153–13161. https://doi.org/10.1021/acs.inorgchem.0c01432.

(22) Bleuzen, A.; Escax, V.; Ferrier, A.; Villain, F.; Verdaguer, M.; Münsch, P.; Itié, J.-P. Thermally Induced Electron Transfer in a CsCoFe Prussian Blue Derivative: The Specific Role of the Alkali-Metal Ion. *Angew. Chem. Int. Ed.* **2004**, *43* (28), 3728–3731. https://doi.org/10.1002/anie.200460086.

(23) Pajerowski, D. M.; Frye, F. A.; Talham, D. R.; Meisel, M. W. Size Dependence of the Photoinduced Magnetism and Long-Range Ordering in Prussian Blue Analogue Nanoparticles of Rubidium Cobalt Hexacyanoferrate. *New J. Phys.* **2007**, *9* (7), 222–222. https://doi.org/10.1088/1367-2630/9/7/222.

(24) Bordage, A.; Moulin, R.; Fonda, E.; Fornasieri, G.; Rivière, E.; Bleuzen, A. Evidence of the Core–Shell Structure of (Photo)Magnetic CoFe Prussian Blue Analogue Nanoparticles and Peculiar Behavior of the Surface Species. *Journal of the American Chemical Society* **2018**, *140* (32), 10332–10343. https://doi.org/10.1021/jacs.8b06147.

(25) Dumont, M. F.; Knowles, E. S.; Guiet, A.; Pajerowski, D. M.; Gomez, A.; Kycia, S. W.; Meisel, M. W.; Talham, D. R. Photoinduced Magnetism in Core/Shell Prussian Blue Analogue Heterostructures of $K_jNi_k[Cr(CN)_6]_l{\cdot}nH_2O$ with $Rb_aCo_b[Fe(CN)_6]_c{\cdot}mH_2O$. *Inorg. Chem.* **2011**, *50* (10), 4295–4300. https://doi.org/10.1021/ic1022054.

(26) Felts, A. C.; Slimani, A.; Cain, J. M.; Andrus, M. J.; Ahir, A. R.; Abboud, K. A.; Meisel, M. W.; Boukheddaden, K.; Talham, D. R. Control of the Speed of a Light-Induced Spin Transition through Mesoscale Core–Shell Architecture. *J. Am. Chem. Soc.* **2018**, *140* (17), 5814–5824. https://doi.org/10.1021/jacs.8b02148.

(27) Nihei, M. Molecular Prussian Blue Analogues: From Bulk to Molecules and Low-Dimensional Aggregates. *Chem. Lett.* **2020**, *49* (10), 1206–1215. https://doi.org/10.1246/cl.200428.

(28) Berlinguette, C. P.; Dragulescu-Andrasi, A.; Sieber, A.; Galán-Mascarós, J. R.; Güdel, H.-U.; Achim, C.; Dunbar, K. R. A Charge-Transfer-Induced Spin Transition in the Discrete Cyanide-Bridged Complex $\{[Co(Tmphen)_2]_3[Fe(CN)_6]_2\}$. *Journal of the American Chemical Society* **2004**, *126* (20), 6222–6223. https://doi.org/10.1021/ja039451k.

(29) Nihei, M.; Sekine, Y.; Suganami, N.; Nakazawa, K.; Nakao, A.; Nakao, H.; Murakami, Y.; Oshio, H. Controlled Intramolecular Electron Transfers in Cyanide-Bridged Molecular Squares by Chemical Modifications and External Stimuli. *Journal of the American Chemical Society* **2011**, *133* (10), 3592–3600. https://doi.org/10.1021/ja109721w.

(30) Zhang, Y.-Z.; Ferko, P.; Siretanu, D.; Ababei, R.; Rath, N. P.; Shaw, M. J.; Clérac, R.; Mathonière, C.; Holmes, S. M. Thermochromic and Photoresponsive Cyanometalate Fe/Co Squares: Toward Control of the Electron Transfer Temperature. *Journal of the American Chemical Society* **2014**, *136* (48), 16854–16864. https://doi.org/10.1021/ja508280n.

(31) Nihei, M.; Shiroyanagi, K.; Kato, M.; Takayama, R.; Murakami, H.; Kera, Y.; Sekine, Y.; Oshio, H. Intramolecular Electron Transfers in a Series of $[Co_2Fe_2]$ Tetranuclear Complexes. *Inorg. Chem.* **2019**, *58* (18), 11912–11919. https://doi.org/10.1021/acs.inorgchem.9b00776.

(32) Nihei, M. Molecular Prussian Blue Analogues: From Bulk to Molecules and Low-Dimensional Aggregates. *Chem. Lett.* **2020**, *49* (10), 1206–1215. https://doi.org/10.1246/cl.200428.

(33) Siretanu, D.; Li, D.; Buisson, L.; Bassani, D. M.; Holmes, S. M.; Mathonière, C.; Clérac, R. Controlling Thermally Induced Electron Transfer in Cyano-Bridged Molecular Squares: From Solid State to Solution. *Chemistry - A European Journal* **2011**, *17* (42), 11704–11708. https://doi.org/10.1002/chem.201102042.

(34) De, S.; Jiménez, J.-R.; Li, Y.; Chamoreau, L.-M.; Flambard, A.; Journaux, Y.; Bousseksou, A.; Lescouëzec, R. One Synthesis: Two Redox States. Temperature-Oriented Crystallization of a Charge Transfer ${$Fe 2 Co 2$}$ Square Complex in a $\{Fe^{II}_{LS}Co^{III}_{LS}\}_2$ Diamagnetic or $\{Fe^{III}_{LS}Co^{II}_{HS}\}_2$ Paramagnetic State. *RSC Advances* **2016**, *6* (21), 17456–17459.

(35) Jiao, C.; Meng, Y.; Yu, Y.; Jiang, W.; Wen, W.; Oshio, H.; Luo, Y.; Duan, C.; Liu, T. Effect of Intermolecular Interactions on Metal- to- Metal Charge Transfer: A Combined Experimental and Theoretical Investigation. *Angew. Chem. Int. Ed.* **2019**, *58* (47), 17009–17015. https://doi.org/10.1002/anie.201909495.

(36) Jiao, C.-Q.; Jiang, W.-J.; Meng, Y.-S.; Wen, W.; Zhao, L.; Wang, J.-L.; Hu, J.-X.; Gurzadyan, G. G.; Duan, C.-Y.; Liu, T. Manipulation of Successive Crystalline Transformations to Control Electron Transfer and Switchable Functions. *National Science Review* **2018**, *5* (4), 507–515. https://doi.org/10.1093/nsr/nwy033.

(37) Nihei, M.; Yanai, Y.; Natke, D.; Takayama, R.; Kato, M.; Sekine, Y.; Renz, F.; Oshio, H. Solid- State Hydrogen- Bond Alterations in a $[Co_2Fe_2]$ Complex with Bifunctional Hydrogen- Bonding Donors. *Chem. Eur. J.* **2019**, *25* (31), 7449–7452. https://doi.org/10.1002/chem.201901383.

(38) Garnier, D.; Jiménez, J.-R.; Li, Y.; von Bardeleben, J.; Journaux, Y.; Augenstein, T.; Moos, E. M. B.; Gamer, M. T.; Breher, F.; Lescouëzec, R. K⊂{$[Fe^{II}(Tp)(CN)_3]_4[Co^{III}(^{pz}Tp)]_3[Co^{II}(^{pz}Tp)]$}: A Neutral Soluble Model Complex of Photomagnetic Prussian Blue Analogues. *Chem. Sci.* **2016**, *7* (8),

4825–4831. https://doi.org/10.1039/C6SC01435F.

(39) Jiménez, J.-R.; Tricoire, M.; Garnier, D.; Chamoreau, L.-M.; Bardeleben, J. von; Journaux, Y.; Li, Y.; Lescouëzec, R. A New {Fe4Co4} Soluble Switchable Nanomagnet Encapsulating Cs+: Enhancing the Stability and Redox Flexibility and Tuning the Photomagnetic Effect. *Dalton Trans.* **2017**, *46* (44), 15549–15557. https://doi.org/10.1039/C7DT02989F.

(40) Daffé, N.; Jiménez, J.-R.; Studniarek, M.; Benchohra, A.; Arrio, M.-A.; Lescouëzec, R.; Dreiser, J. Direct Observation of Charge Transfer and Magnetism in Fe_4Co_4 Cyanide-Bridged Molecular Cubes. *J. Phys. Chem. Lett.* **2019**, *10* (8), 1799–1804. https://doi.org/10.1021/acs.jpclett.8b03839.

(41) Xuan, Q. P.; Glatz, J.; Benchohra, A.; Jiménez, J.-R.; Plamont, R.; Chamoreau, L.-M.; Flambard, A.; Li, Y.; Lisnard, L.; Dambournet, D.; Borkiewicz, O. J.; Boillot, M.-L.; Catala, L.; Tissot, A.; Lescouëzec, R. Building Responsive Materials by Assembling $\{Fe_4Co_4\}$ Switchable Molecular Cubes. *J. Mater. Chem. C* **2021**, *9* (28), 8882–8890. https://doi.org/10.1039/D1TC01825F.

(42) Klausmeyer, K. K.; Wilson, S. R.; Rauchfuss, T. B. Alkali Metal-Templated Assembly of Cyanometalate "boxes" (NEt4)3{M[Cp*Rh(Cn)3]4[Mo(CO)3]4} (M = K, Cs). Selective Binding of Cs+. *Journal of the American Chemical Society* **1999**, *121* (12), 2705–2711. https://doi.org/10.1021/ja982347w.

(43) Heinrich, J. L.; Berseth, P. A.; Long, J. R. Molecular Prussian Blue Analogues: Synthesis and Structure of Cubic Cr4Co4(CN)12 and Co8(CN)12 Clusters. *Chemical Communications* **1998**, *4*, 1231–1232. https://doi.org/10.1039/a802351d.

(44) Li, D.; Clérac, R.; Roubeau, O.; Harté, E.; Mathonière, C.; Le Bris, R.; Holmes, S. M. Magnetic and Optical Bistability Driven by Thermally and Photoinduced Intramolecular Electron Transfer in a Molecular Cobalt−Iron Prussian Blue Analogue. *J. Am. Chem. Soc.* **2008**, *130* (1), 252–258. https://doi.org/10.1021/ja0757632.

(45) Mondal, A.; Li, Y.; Seuleiman, M.; Julve, M.; Toupet, L.; Buron-Le Cointe, M.; Lescouëzec, R. On/Off Photoswitching in a Cyanide-Bridged $\{Fe_2Co_2\}$ Magnetic Molecular Square. *Journal of the American Chemical Society* **2013**, *135* (5), 1653–1656. https://doi.org/10.1021/ja3087467.

(46) Granier, T.; Galloislc, B. 1,4,5,8-Tetraazaphenanthrene; *Inorg. Chem.* **1994**, *33* (6), 3587.

(47) Wei, R.-J.; Nakahara, R.; Cameron, J. M.; Newton, G. N.; Shiga, T.; Sagayama, H.; Kumai, R.; Murakami, Y.; Oshio, H. Solvent-Induced on/off Switching of Intramolecular Electron Transfer in a Cyanide-Bridged Trigonal Bipyramidal Complex. *Dalton Trans.* **2016**, *1*, 1–4. https://doi.org/10.1039/C6DT03416K.

(48) Wei, R.; Shiga, T.; Newton, G. N.; Robinson, D.; Takeda, S.; Oshio, H. A Cyanide-Bridged Magnetically Switchable Cage with Encapsulated Water Molecules. **2016**, 10–13. https://doi.org/10.1021/acs.inorgchem.6b02306.

(49) Mondal, A. Switchable Molecular Magnetic Materials, PhD. Thesis, Université Pierre et Marie Curie, Paris, **2013**.

(50) Bridonneau, N.; Rigamonti, L.; Poneti, G.; Pinkowicz, D.; Forni, A.; Cornia, A. Evidence of Crystal Packing Effects in Stabilizing High or Low Spin States of Iron(<scp>ii</Scp>) Complexes with Functionalized 2,6-Bis(Pyrazol-1-Yl)Pyridine Ligands. *Dalton Trans.* **2017**, *46* (12), 4075–4085. https://doi.org/10.1039/C7DT00248C.

(51) S. De; Jiménez J.-R., Li, Y., Chamoreau, L.-M., Flambard, A., Journaux, Y., Bousseksou, A., Lescouëzec, R., S. One Synthesis: Two Redox States. Temperature-Oriented Crystallization of a Charge Transfer {Fe2Co2} Square Complex in a {FeLS IICoLS III}2 Diamagnetic or $\{Fe_{LS}^{III}Co_{HS}^{II}{}_2$ Paramagnetic State. *RSC Advances* **2016**, *6*, 17456–17459. https://doi.org/10.1039/c6ra00191b.

(52) Mercurol, J.; Li, Y.; Pardo, E.; Risset, O.; Seuleiman, M.; Rousselière, H.; Lescouëzec, R.; Julve, M. [FeIILSCoIIILS]2⇔ [FeIIILSCoIIHS]2 Photoinduced Conversion in a Cyanide-Bridged Heterobimetallic Molecular Square. *Chemical Communications* **2010**, *46* (47), 8995. https://doi.org/10.1039/c0cc02024a.

(53) Pardo, E.; Verdaguer, M.; Herson, P.; Rousselière, H.; Cano, J.; Julve, M.; Lloret, F.; Lescouëzec, R. Synthesis, Crystal Structures, and Magnetic Properties of a New Family of Heterometallic Cyanide-Bridged $Fe^{III}{}_2M^{II}{}_2$ (M = Mn, Ni, and Co) Square Complexes. *Inorganic Chemistry* **2011**, *50* (13), 6250–6262. https://doi.org/10.1021/ic200616p.

(54) Chastanet, G.; Lorenc, M.; Bertoni, R.; Desplanches, C. Light-Induced Spin Crossover—Solution and Solid-State Processes. *Comptes Rendus Chimie* **2018**, *21* (12), 1075–1094. https://doi.org/10.1016/j.crci.2018.02.011.

(55) Gütlich, P.; Hauser, A. Thermal and Light-Induced Spin Crossover in Iron(II) Complexes. *Coordination Chemistry Reviews* **1990**, *97*, 1–22. https://doi.org/10.1016/0010-8545(90)80076-6.

(56) Gütlich, P.; Goodwin, H. A. *Spin Crossover in Transition Metal Compounds II*; Topics in Current Chemistry; Springer Berlin Heidelberg: Berlin, Heidelberg, 2004; Vol. 234. https://doi.org/10.1007/b93641.

(57) Lloret, F.; Julve, M.; Cano, J.; Ruiz-García, R.; Pardo, E. Magnetic Properties of Six-Coordinated High-Spin Cobalt(II) Complexes: Theoretical Background and Its Application. *Inorganica Chimica Acta* **2008**, *361* (12–13), 3432–3445. https://doi.org/10.1016/j.ica.2008.03.114.

(58) Létard, J.-F. Photomagnetism of Iron(II) Spin Crossover Complexes—the T(LIESST) Approach. *J. Mater. Chem.* **2006**, *16* (26), 2550–2559. https://doi.org/10.1039/B603473J.

(59) Hauser, A. Intersystem Crossing in Fe(II) Coordination Compounds. *Coordination Chemistry Reviews*. Amsterdam 1991, pp 275–290.

(60) Guo, Y.-N.; Xu, G.-F.; Guo, Y.; Tang, J. Relaxation Dynamics of Dysprosium(Iii) Single Molecule Magnets. *Dalton Trans.* **2011**, *40* (39), 9953. https://doi.org/10.1039/c1dt10474h.

(61) Li, D.; Clérac, R.; Roubeau, O.; Harté, E.; Mathonière, C.; Le Bris, R.; Holmes, S. M. Magnetic and Optical Bistability Driven by Thermally and Photoinduced Intramolecular Electron Transfer in a Molecular Cobalt−Iron Prussian Blue Analogue. *J. Am. Chem. Soc.* **2008**, *130* (1), 252–258. https://doi.org/10.1021/ja0757632.

(62) Varret, F.; Boukheddaden, K.; Codjovi, E.; Maurin, I.; Tokoro, H.; Ohkoshi, S.; Hashimoto, K. Light-Induced Thermal Hysteresis and Intensity Thresholds in Molecular Switcheable Solids, by Mean-Field Macroscopic Master Equation Approach: Discussion of the Experimental Data Obtained for Co–Fe Prussian Blue Analogues. *Polyhedron* **2005**, *24* (16–17), 2857–2863. https://doi.org/10.1016/j.poly.2005.06.013.

(63) Gawali-Salunke, S.; Varret, F.; Maurin, I.; Enachescu, C.; Malarova, M.; Boukheddaden, K.; Codjovi, E.; Tokoro, H.; Ohkoshi, S.; Hashimoto, K. Magnetic and Mössbauer Investigation of the Photomagnetic Prussian Blue Analogue $Na_{0.32}Co[Fe(CN)_6]_{0.74} \cdot 3.4H_2O$: Cooperative Relaxation of the Thermally Quenched State. *J. Phys. Chem. B* **2005**, *109* (16), 8251–8256. https://doi.org/10.1021/jp044739x.

(64) Cafun, J.-D.; Lejeune, J.; Baudelet, F.; Dumas, P.; Itié, J.-P.; Bleuzen, A. Room-Temperature Photoinduced Electron Transfer in a Prussian Blue Analogue under Hydrostatic Pressure. *Angew. Chem. Int. Ed.* **2012**, *51* (36), 9146–9148. https://doi.org/10.1002/anie.201203943.

(65) Baldé, C.; Sylla, M. S.; Desplanches, C.; Chastanet, G. High-Spin → Low-Spin Relaxation Kinetics and Metal Dilution Effects in 1D Spin-Crossover Chain Compounds. *Polyhedron* **2019**, *159*, 84–92. https://doi.org/10.1016/j.poly.2018.11.046.

(66) Mathonière, C. Metal-to-Metal Electron Transfer: A Powerful Tool for the Design of Switchable Coordination Compounds: Metal-to-Metal Electron Transfer: A Powerful Tool for the Design of Switchable Coordination Compounds. *European Journal of Inorganic Chemistry* **2018**, *2018* (3–4), 248–258. https://doi.org/10.1002/ejic.201701194.

(67) Hauser, A. Intersystem Crossing in Fe(II) Coordination Compounds. *Coordination Chemistry Reviews* **1991**, *111*, 275–290. https://doi.org/10.1016/0010-8545(91)84034-3.

(68) Hogue, R. W.; Singh, S.; Brooker, S. Spin Crossover in Discrete Polynuclear Iron(II) Complexes. *Chem. Soc. Rev.* **2018**, *47* (19), 7303–7338. https://doi.org/10.1039/C7CS00835J.

(69) Létard, J.-F.; Chastanet, G.; Nguyen, O.; Marcén, S.; Marchivie, M.; Guionneau, P.; Chasseau, D.; Gütlich, P. Spin Crossover Properties of the $[Fe(PM\text{-}BiA)_2(NCS)_2]$ Complex - Phases I and II. *Monatshefte für Chemie / Chemical Monthly* **2003**, *134* (2), 165–182. https://doi.org/10.1007/s00706-002-0537-0.

(70) Baldé, C.; Paradis, N.; Desplanches, C.; Chastanet, G. Switchable Heteroleptic Mononuclear Iron(II) Complexes as Versatile Molecular Building Block: Switchable Heteroleptic Mononuclear Iron(II) Complexes as Versatile Molecular Building Block. *Eur. J. Inorg. Chem.* **2018**, *2018* (19), 2004–2010. https://doi.org/10.1002/ejic.201800053.

(71) Henstridge, M. C.; Laborda, E.; Rees, N. V.; Compton, R. G. Marcus–Hush–Chidsey Theory of Electron Transfer Applied to Voltammetry: A Review. *Electrochimica Acta* **2012**, *84*, 12–20. https://doi.org/10.1016/j.electacta.2011.10.026.

(72) Savéant, J.-M. *Elements of Molecular and Biomolecular Electrochemistry: An Electrochemical Approach to Electron Transfer Chemistry*; John Wiley & Sons, Inc.: Hoboken, NJ, USA, 2006. https://doi.org/10.1002/0471758078.

(73) De Alwis, D. C. L.; Schultz, F. A. Metal−Bis[Poly(Pyrazolyl)Borate] Complexes. Electrochemical, Magnetic, and Spectroscopic Properties and Coupled Electron-Transfer and Spin-Exchange Reactions. *Inorg. Chem.* **2003**, *42* (11), 3616–3622. https://doi.org/10.1021/ic034077a.

(74) Turner, J. W.; Schultz, F. A. Electrochemical Activation Parameters of Coupled Electron-Transfer and Spin-Exchange Reactions. Experimental Studies of $[M(Tacn)_2]^{3+/2+}$ and $[Fe(Pzb)_2]^{+/0}$ Redox Systems. *J. Phys. Chem. B* **2002**, *106* (8), 2009–2017. https://doi.org/10.1021/jp013294z.

(75) Sheets, J. R.; Schultz, F. A. Coupled Electron-Transfer and Spin-Exchange Reactions of Metal–Bis[Tris(Pyrazolyl)Methane] Complexes. *Polyhedron* **2004**, *23* (6), 1037−1043. https://doi.org/10.1016/j.poly.2004.01.004.

(76) Chastanet, G.; Desplanches, C.; Baldé, C.; Rosa, P.; Marchivie, M.; Guionneau, P. A Critical Review of the T(LIESST) Temperature in Spin Crossover Materials − What It Is and What It Is Not. *Chem.Sq.* **2018**. https://doi.org/10.28954/2018.csq.07.001.

(77) Tumanov, S. V.; Veber, S. L.; Tolstikov, S. E.; Artiukhova, N. A.; Romanenko, G. V.; Ovcharenko, V. I.; Fedin, M. V. Light-Induced Spin State Switching and Relaxation in Spin Pairs of Copper(II)–Nitroxide Based Molecular Magnets. *Inorg. Chem.* **2017**, *56* (19), 11729–11737. https://doi.org/10.1021/acs.inorgchem.7b01689.

(78) Hauser, A.; Enachescu, C.; Daku, M. L.; Vargas, A.; Amstutz, N. Low-Temperature Lifetimes of Metastable High-Spin States in Spin-Crossover and in Low-Spin Iron(II) Compounds: The Rule and Exceptions to the Rule. *Coordination Chemistry Reviews* **2006**, *250* (13–14), 1642–1652. https://doi.org/10.1016/j.ccr.2005.12.006.

(79) Stock, P.; Deck, E.; Hohnstein, S.; Korzekwa, J.; Meyer, K.; Heinemann, F. W.; Breher, F.; Hörner, G. Molecular Spin Crossover in Slow Motion: Light-Induced Spin-State Transitions in Trigonal Prismatic Iron(II) Complexes. *Inorg. Chem.* **2016**, *55* (11), 5254–5265. https://doi.org/10.1021/acs.inorgchem.6b00238.

(80) Buron-Le Cointe, M.; Hébert, J.; Baldé, C.; Moisan, N.; Toupet, L.; Guionneau, P.; Létard, J. F.; Freysz, E.; Cailleau, H.; Collet, E. Intermolecular Control of Thermoswitching and Photoswitching Phenomena in Two Spin-Crossover Polymorphs. *Phys. Rev. B* **2012**, *85* (6), 064114. https://doi.org/10.1103/PhysRevB.85.064114.

(81) Marchivie, M.; Guionneau, P.; Létard, J.-F.; Chasseau, D. Photo-Induced Spin-Transition: The Role of the Iron(II) Environment Distortion. *Acta Crystallogr B Struct Sci* **2005**, *61* (1), 25–28. https://doi.org/10.1107/S0108768104029751.

(82) Lejeune, J.; Cafun, J.-D.; Fornasieri, G.; Brubach, J.-B.; Creff, G.; Roy, P.; Bleuzen, A. Microscopic Origin for Multistability in a Photomagnetic CoFe Prussian Blue Analogue. *Eur. J. Inorg. Chem.* **2012**, *2012* (25), 3980–3983. https://doi.org/10.1002/ejic.201200746.

(83) Létard, J.-F. Photomagnetism of Iron(Ii) Spin Crossover Complexes—the T (LIESST) Approach. *Journal of Materials Chemistry* **2006**, *16* (26), 2550–2559. https://doi.org/10.1039/B603473J.

Table of Contents artwork